



**HAL**  
open science

# A proxy modelling approach to assess the potential of extracting ENSO signal from tropical Pacific planktonic foraminifera

Brett Metcalfe, Bryan C. Lougheed, Claire Waelbroeck, Didier M. Roche

► **To cite this version:**

Brett Metcalfe, Bryan C. Lougheed, Claire Waelbroeck, Didier M. Roche. A proxy modelling approach to assess the potential of extracting ENSO signal from tropical Pacific planktonic foraminifera. *Climate of the Past*, 2020, 16 (3), pp.885-910. 10.5194/cp-16-885-2020 . hal-02766071

**HAL Id: hal-02766071**

**<https://hal.science/hal-02766071>**

Submitted on 10 Jun 2020

**HAL** is a multi-disciplinary open access archive for the deposit and dissemination of scientific research documents, whether they are published or not. The documents may come from teaching and research institutions in France or abroad, or from public or private research centers.

L'archive ouverte pluridisciplinaire **HAL**, est destinée au dépôt et à la diffusion de documents scientifiques de niveau recherche, publiés ou non, émanant des établissements d'enseignement et de recherche français ou étrangers, des laboratoires publics ou privés.



Distributed under a Creative Commons Attribution 4.0 International License



# A proxy modelling approach to assess the potential of extracting ENSO signal from tropical Pacific planktonic foraminifera

Brett Metcalfe<sup>1,2</sup>, Bryan C. Lougheed<sup>1,3</sup>, Claire Waelbroeck<sup>1</sup>, and Didier M. Roche<sup>1,2</sup>

<sup>1</sup>Laboratoire des Sciences du Climat et de l'Environnement, LSCE/IPSL, CEA–CNRS–UVSQ, Université Paris-Saclay, 91191 Gif-sur-Yvette, France

<sup>2</sup>Earth and Climate Cluster, Department of Earth Science, Faculty of Science, Vrije Universiteit Amsterdam, de Boelelaan 1085, 1081 HV, Amsterdam, the Netherlands

<sup>3</sup>Department of Earth Sciences, Uppsala University, Villavägen 16, 75236 Uppsala, Sweden

**Correspondence:** Brett Metcalfe (brett\_metcalfe@outlook.com)

Received: 21 January 2019 – Discussion started: 1 March 2019

Revised: 21 February 2020 – Accepted: 28 February 2020 – Published: 20 May 2020

**Abstract.** A complete understanding of past El Niño–Southern Oscillation (ENSO) fluctuations is important for the future predictions of regional climate using climate models. One approach to reconstructing past ENSO dynamics uses planktonic foraminifera as recorders of past climate to assess past spatio-temporal changes in upper ocean conditions. In this paper, we utilise a model of planktonic foraminifera populations, Foraminifera as Modelled Entities (FAME), to forward model the potential monthly average  $\delta^{18}\text{O}_c$  and temperature signal proxy values for *Globigerinoides ruber*, *Globigerinoides sacculifer*, and *Neoglobobulimina dutertrei* from input variables covering the period of the instrumental record. We test whether the modelled foraminifera population  $\delta^{18}\text{O}_c$  and  $T_c$  associated with El Niño events statistically differ from the values associated with other climate states. Provided the assumptions of the model are correct, our results indicate that the values of El Niño events can be differentiated from other climate states using these species. Our model computes the proxy values of foraminifera in the water, suggesting that, in theory, water locations for a large portion of the tropical Pacific should be suitable for differentiating El Niño events from other climate states. However, in practice it may not be possible to differentiate climate states in the sediment record. Specifically, comparison of our model results with the sedimentological features of the Pacific Ocean shows that a large portion of the hydrographically/ecologically suitable water regions coincide with low sediment accumulation rate at the sea floor

and/or of sea floor that lie below threshold water depths for calcite preservation.

## 1 Introduction

### 1.1 El Niño–Southern Oscillation (ENSO)

Predictions of short-term, abrupt changes in regional climate are imperative for improving spatio-temporal precision and accuracy when forecasting future climate. Coupled ocean–atmosphere interactions (wind circulation and sea surface temperature) in the tropical Pacific, collectively known as the El Niño–Southern Oscillation (ENSO) on interannual timescales and the Pacific Decadal Oscillation on decadal timescales, represent largest source of interannual climate variability in global climate (Wang et al., 2017). Due to ENSO's major socioeconomic impacts upon pan-Pacific nations, which, depending on the location, can include flooding, drought, and fire risk, it is imperative to have an accurate understanding of both past and future behaviour of ENSO (Trenberth and Otto-Bliesner, 2003; Rosenthal and Broccoli, 2004; McPhaden et al., 2006). The instrumental record of the past century provides important information (that can be translated into the Southern Oscillation Index; SOI); however, detailed oceanographic observations of the components of ENSO (both the El Niño and Southern Oscillation), such as the Tropical Oceans Global Atmosphere (TOGA; 1985–1994) experiment only provide information from the latter half of the twentieth century (Wang et al., 2017). To ac-

quire longer records, researchers must turn to the geological record using various archives that are available from the (pan-)Pacific region. An integrated approach combining palaeoclimate proxies (Ford et al., 2015; de Garidel-Thoron et al., 2007; Koutavas et al., 2006; Koutavas and Joanides, 2012; Koutavas and Lynch-Stieglitz, 2003; Leduc et al., 2009; White et al., 2018) and computer models (Zhu et al., 2017) can help shed light on the triggers of past ENSO events, their magnitude, and their spatio-temporal distribution.

## 1.2 Foraminiferal proxies

The simulation of past ENSO using climate models has been fraught with difficulties due to ENSO's integration into the climate system and the associated feedbacks of ENSO upon model boundary conditions (e.g. sea surface temperature – SST – and  $p\text{CO}_2$ ) (Ford et al., 2015). One way to deduce the relative impact and importance of various feedbacks and, in turn, reduce model-dependent noise in our predictions, is to compare model output with proxy data such as foraminifera. Such an approach, however, requires an abundance of reliable spatio-temporal proxy data for the entire Pacific Ocean. The reliability of proxy reconstructions are themselves subject to several unknowns, uncertainties and biases. For instance culture experiments have identified temperature (Lombard et al., 2009, 2011), light (Bé et al., 1982; Bé and Spero, 1981; Lombard et al., 2010; Rink et al., 1998; Spero and DeNiro, 1987; Wolf-Gladrow et al., 1999), carbonate ion concentration ( $[\text{CO}_3^{2-}]$ ) (Bijma et al., 2002; Lombard et al., 2010), and ontogenetic changes (Hamilton et al., 2008; Wycech et al., 2018) as variables that drive, alter, or induce changes in foraminiferal growth. These variables are important as foraminifera are not passive recorders of environmental conditions such as SST, in that the very same ambient environment that researchers wish to reconstruct can modify the foraminiferal population (Mix, 1987; Mulitza et al., 1998). Sensitivity to the variable being reconstructed may increase or decrease the relative contribution of individual ENSO events, due to modulation of the flux to the seafloor, increasing or decreasing the chance of sampling such occurrences, etc. (Mix, 1987; Mulitza et al., 1998). Computation of the influence of biological and vital effects upon physiochemical proxies, such as those based on foraminifera should be a fundamental consideration for any accurate data–model comparison. Recent attempts at circumnavigating proxy-related problems have employed isotope-enabled models (Caley et al., 2014; Roche et al., 2014; Zhu et al., 2017), proxy system models (Evans et al., 2013; Dolman and Laepple, 2018; Jonkers and Kučera, 2017; Roche et al., 2018) or uncertainty analysis (Thirumalai et al., 2013; Fraass and Lowery, 2017; Dolman and Laepple, 2018) to predict both the potential  $\delta^{18}\text{O}_c$  values in foraminifera and/or the probability of detection of a climatic event. The use of eco-physiological models (Kageyama et al., 2013; Lombard et

al., 2009, 2011) can help circumvent some of the problems associated with a purely mathematical approximation (e.g. Caley et al., 2014) of the translation of an ambient signal into a palaeoclimate proxy. They are not limited to foraminifera and can provide an important way to test whether proxies used for palaeoclimate reconstructions are suitable for the given research question. Several studies have investigated the response of planktonic foraminifera from core material or computed pseudo foraminiferal distributions, their proxy values, and the resultant (likely) distribution of these proxy values with respect to ENSO (e.g. Leduc et al., 2009; Thirumalai et al., 2013; Ford et al., 2015; Zhu et al., 2017).

## 1.3 Aims and objectives

Here, we investigate whether living planktonic foraminifera can be theoretically used in ENSO reconstructions, differing from previous research (e.g. Thirumalai et al., 2013) by using a foraminiferal growth model, Foraminifera as Modelled Entities (FAME; Roche et al., 2018), to tackle the dynamic seasonal and depth habitat of planktonic foraminifera (Wilke et al., 2006; Steinhardt et al., 2015; Mix, 1987; Mulitza et al., 1998). To be a useful proxy for the reconstruction of ENSO, the resulting proxy values of populations of planktonic foraminifera associated with different climatic states (i.e. El Niño, neutral, or La Niña) should be significantly different from one another. In order to test our research question, “are the distributions of proxy values associated with El Niño months statistically different from distributions of proxy values associated with neutral or La Niña months?”, our methodology follows a forward modelling approach in which the computed values of the temperature recorded by calcite ( $T_c$  – a pseudo temperature aimed at mimicking Mg/Ca) and  $\delta^{18}\text{O}_c$  are assigned to one of these climatological states. This forward modelling approach does not presuppose foraminifera can record ENSO variability (i.e. it asks, “Can we detect?”), which is done by inverting the core top pooled  $\delta^{18}\text{O}$  or individual foraminiferal  $\delta^{18}\text{O}$  distributions and using measured values to infer changes in ENSO (“How could we detect?”). Whilst we are principally interested in understanding whether living foraminifera can theoretically reconstruct ENSO (Sects. 4 and 5), comparison with data requires further analysis. A secondary objective is to compare the output of this approach with secondary factors that further modulate the climatic signal through postmortem processes. If the foraminifera modulate the original climate signal, then preservation selectively filters which specimens are conserved, and bioturbation acts to reorder, thus scrambling the stratigraphic order in which they are recorded by the sediment depth domain, such that the stratigraphic order is no longer directly equivalent to the time domain. Once the sediment is recovered, the researcher acts as a final filter, which is in essence a random picking process (Sect. 6). We identify regions in the Pacific Ocean where the sedimentation rate may be too low or the water depth too deep (causing dissolution

of carbonate sediments) thus potentially preventing the capture and preservation of the foraminiferal signal (Sect. 7). To aid the reader, only the general methodology is outlined in Sect. 2, with the individual methodologies of each objective (referred to as Experiments 1 to 5) defined in each subsequent section (Sects. 3 to 7).

## 2 General methodology

### 2.1 Input variables (temperature, salinity, $\delta^{18}\text{O}_{\text{sw}}$ , and $\delta^{18}\text{O}_{\text{eq}}$ )

For input variables, temperature, and salinity of the ocean reanalysis data product (Universität, Hamburg, DE) ORAS4 (Balmaseda et al., 2013) were extracted at  $1^\circ$  resolution for the tropical Pacific ( $-20^\circ\text{S}$  to  $20^\circ\text{N}$  and  $120^\circ\text{E}$  to  $-70^\circ\text{W}$ ), with each single grid cell comprised of data from 42 depth intervals (5–5300 m water depth) and 696 months (January 1958–December 2015). For computation of the oxygen isotope of seawater ( $\delta^{18}\text{O}_{\text{sw}}$ ), a global  $1^\circ$  grid was generated, and each grid cell was classified as belonging to one of 27 distinct ocean regions, as defined by either societal or scientific agencies. For identifying regional  $\delta^{18}\text{O}_{\text{sw}}$ –salinity relationships (LeGrande and Schmidt, 2006). Using the  $\delta^{18}\text{O}_{\text{sw}}$  database of LeGrande and Schmidt (2006) a regional  $\delta^{18}\text{O}_{\text{sw}}$ –salinity relationship was defined, in which the salinity is the salinity measured directly at the isotope sample collection point (included within the database). Two matrices were computed; one giving values of the slope ( $m$ ) and the other of intercept ( $c$ ) of the resultant linear regression equations, and these were used as look-up tables to define the monthly  $\delta^{18}\text{O}_{\text{sw}}$  from the monthly salinity ocean reanalysis product ORAS4 (Balmaseda et al., 2013), which was used for the calculation of  $\delta^{18}\text{O}_{\text{eq}}$ ; i.e. the expected  $\delta^{18}\text{O}$  for foraminiferal calcite formed at a certain temperature (Kim and O’Neil, 1997). The  $\delta^{18}\text{O}_{\text{eq}}$  is calculated from a rearranged form of the following temperature equation:

$$T = T_0 - b \cdot (\delta^{18}\text{O}_c - \delta^{18}\text{O}_{\text{sw}}) + a \cdot (\delta^{18}\text{O}_c - \delta^{18}\text{O}_{\text{sw}})^2. \quad (1)$$

Specifically, we used the quadratic approximation (Bemis et al., 1998) of Kim and O’Neil (1997), where  $T_0 = 16.1$ ,  $a = 0.09$ ,  $b = 4.64$ , and it is converted from V-SMOW to V-PDB using a constant of  $-0.27\text{‰}$  (Hut, 1987; Roche et al., 2018) as follows:

$$\Delta = b^2 - 4a \cdot (T_0 - T_{\text{sw}}), \quad (2)$$

$$\delta^{18}\text{O}_{c, \text{eq}} = \frac{-b - \sqrt{\Delta}}{2a} + \delta^{18}\text{O}_{\text{sw}} - 0.27. \quad (3)$$

The dynamic value of Brand et al. (2014) is not used.

### 2.2 Climate classification

Pan-Pacific meteorological agencies differ in their definition of an El Niño (An and Bong, 2016, 2018), with the

definition of each country reflecting socioeconomic factors. Therefore, for simplicity we use the Oceanic Niño Index (ONI), based upon the Niño 3.4 region ( $5^\circ\text{N}$  to  $-5^\circ\text{S}$ ,  $170^\circ\text{E}$  to  $120^\circ\text{W}$ ; Fig. S1 in the Supplement) because of the importance of the region for interactions between ocean and atmosphere, which is a 3-month running mean of SST anomalies in ERSST.v5 (Huang et al., 2017). We utilise a threshold of  $\chi \geq +0.5^\circ\text{C}$  (where  $\chi$  is the value of ONI) as a proxy for El Niño,  $-0.5^\circ\text{C} \leq \chi \leq +0.5^\circ\text{C}$  for neutral climate conditions, and  $\chi \leq -0.5^\circ\text{C}$  for a La Niña in the Oceanic Niño Index. Many meteorological agencies consider that 5 consecutive months of  $\chi \geq +0.5^\circ\text{C}$  must occur for the classification of an El Niño event. However, here the only difference is that we consider that any single month falling within our threshold values as representative of El Niño, neutral, or La Niña conditions (grey bars in Fig. S1). This simplification reflects the life cycle of planktonic foraminifera ( $\sim 4$  weeks) seeing that the population at time step  $t$  does not record what happened at  $t - 1$  or what will happen at  $t + 1$ . As we are producing the mean population-growth-weighted  $\delta^{18}\text{O}$  values, the periods when the ONI threshold is exceeded but an El Niño or La Niña event does not occur (i.e. an “almost” El Niño or ‘almost’ La Niña) would be indistinguishable from the build-up and subsequent climb-down of actual El Niño and La Niña events when the foraminiferal values are pooled in the sediment. Therefore, these “almost” El Niño or “almost” La Niña (months that exceed the threshold) are placed within their respective climatological pools as El Niño or La Niña.

Each time step for the entirety of the Pacific was classified as one of three climate states (El Niño, neutral, and La Niña), and the corresponding values at each time step were binned into their respective categories for each grid point. The binned values are either the input data (Sect. 3: Experiment 1) or the  $\delta^{18}\text{O}_c$  and  $T_c$  produced by FAME (Sect. 4: Experiment 2). An Epanechnikov-kernel distribution was first fitted to the binned monthly output of a single climate state (using the fit distribution function `fitdist` of MATLAB); the bandwidth varies between grid points to provide for an optimal kernel distribution (applying the default option of the function in MATLAB). The use of a nonparametric representation (i.e. the kernel distribution) to fit the data, as opposed to other types of distribution (e.g. Gaussian), represents a trade-off between keeping as many parameters constant, mimicking the underlying dataset for a large number of grid points and avoiding making too many assumptions regarding the structure of the underlying data. The conversion of the data from dataset to distribution may induce some small error by the following: rounding to whole integers; the use of a  $\delta^{18}\text{O}_{\text{midpoint}}$  which gives an error associated with the bin size ( $\pm 0.05\text{‰}$ ) that is symmetrical close to the distributions measures of central tendency but asymmetrical at the sides; and finally, the associated rounding error at the bin edges within a histogram ( $\pm 0.005\text{‰}$ ). Subsequently, the shape of any two desired distributions can be compared for

statistically significant (dis)similarity using an Anderson–Darling test (Anderson and Darling, 1954). For each test, a comparison is made between all the values of one climatological state and all the values of another climatological state.

### 3 Experiment 1: input parameters

#### 3.1 Objective

The resultant values produced by FAME are a modulation of the original input climate signal; therefore it is important to determine to what extent our model has altered the signal and if interpretations we garner from FAME depend upon the models growth rates values (Roche et al., 2018). In Experiment 1 we use a basin-wide statistical test to examine whether the temperature or  $\delta^{18}\text{O}_{\text{eq}}$  values used as input in FAME for a given El Niño population and a given non-El Niño (neutral conditions) population can be expected to be significantly different at any given specific location. Where the two populations exhibit significantly different distributions, ENSO events can potentially be detected by palaeoceanographers. However, where the populations do not exhibit significantly different values, then the location represents a poor choice to study ENSO dynamics.

#### 3.2 Methodology (temperature and calculated $\delta^{18}\text{O}_{\text{eq}}$ )

The input datasets of temperature and calculated  $\delta^{18}\text{O}_{\text{eq}}$  underwent the following statistical test (Fig. 1): for each grid point and for every time step, values were extracted from fixed depths of 5, 149, and 235 m (Fig. S2). These selected values from discrete-depth intervals were placed into their climatological classifications, and the resultant climatic distributions were compared with one another using an Anderson–Darling test in order to compare the (dis)similarity of the resultant climatic distributions. Unlike FAME, which integrates over several depth levels using the computed growth rate, the test of the input datasets was with fixed depths without any growth rate weighting, in order to observe the implications of FAME's dynamic depth habitat. The threshold errors (i.e. the difference between the means of each distribution) are  $0.5\text{ }^{\circ}\text{C}$  for temperature (Fig. 1a) and  $0.10\text{ }_{\text{‰}}$  for  $\delta^{18}\text{O}_{\text{eq}}$  (Fig. 1b); these errors should be viewed as a guide rather than an implicit rejection of a site.

#### 3.3 Results and discussion

The results of the Anderson–Darling test performed on the underlying input dataset (temperature and  $\delta^{18}\text{O}_{\text{eq}}$ ) for each grid point are presented as black, grey, or hashed. Areas where the population distributions of the two climate states are found to be statistically similar have black grid cells. Regions in which the difference between the two populations are larger than the potential error are associated with grey, whereas the regions with differences less than the potential

error are represented as hashed regions (Fig. 1). The results of this fixed depth, non-FAME, test show that the shallowest depths produce populations that are significantly different both in terms of their mean values and their distributions and are thus suitable water locations for recording ENSO dynamics. In Fig. 1a, the canonical El Niño 3.4 region is clearly visible at 5 m depth, though there are marked differences and similarities between the Anderson–Darling results for the various other depths of the input data (see Fig. S2).

### 4 Experiment 2: Foraminifera as Modelled Entities (FAME)

#### 4.1 Objective

In Experiment 2 we run FAME on our two input datasets (temperature and oxygen isotope equilibrium). Data–model comparison studies suffer from an inability to directly compare like with like due to differences in the following: (i) the units used; i.e. most proxies reconstructing temperature do not directly give values of temperature in degrees Celsius or kelvin but in their own proxy units (e.g.  $\text{‰}$ , per mil;  $\text{mmol mol}^{-1}$ ; and species abundance or ratio) necessitating a conversion; and (ii) scales in the time–depth domain; i.e. models give a wealth of information (multiple depth layers and high resolution time slices). Foraminifera as Modelled Entities (FAME) was developed as an attempt to reduce the error associated with data–model comparisons (i) by generating simulated-proxy time series from a climatic input (a reanalysis dataset or climate model output) that can be compared with age–depth values down core; and (ii) to reduce the model information for a given time slice into a manageable and relevant value using an integration that would make sense from a biological point of view (Roche et al., 2018), approximating the depth integrated growth of foraminifera (e.g. Pracht et al., 2019; Wilke et al., 2006; Steinhardt et al., 2015). FAME uses the temperature and  $\delta^{18}\text{O}_{\text{eq}}$  profiles at each grid cell to compute a time-averaged  $\delta^{18}\text{O}_{\text{c}}$  and  $T_{\text{c}}$  for a given species. Using a basin-wide statistical test, we examine whether the  $\delta^{18}\text{O}_{\text{c}}$  values of a given El Niño foraminifera population ( $\text{FP}_{\text{EN}}$ ) and a given non-El Niño (neutral conditions) foraminifera population ( $\text{FP}_{\text{NEU}}$ ) can be expected to be significantly different at any given specific location. Where  $\text{FP}_{\text{EN}}$  and  $\text{FP}_{\text{NEU}}$  exhibit significantly different distributions, ENSO events can potentially be detected by palaeoceanographers. In cases where  $\text{FP}_{\text{EN}}$  and  $\text{FP}_{\text{NEU}}$  do not exhibit significantly different values, then the chosen species and/or location represent a poor choice to study ENSO dynamics.

#### 4.2 Methodology

##### 4.2.1 FAME Model

The FAME model utilises the temperature–growth rate equations of Lombard et al. (2009) to simulate temperature-derived growth rate (Kageyama et al., 2013; Lombard et

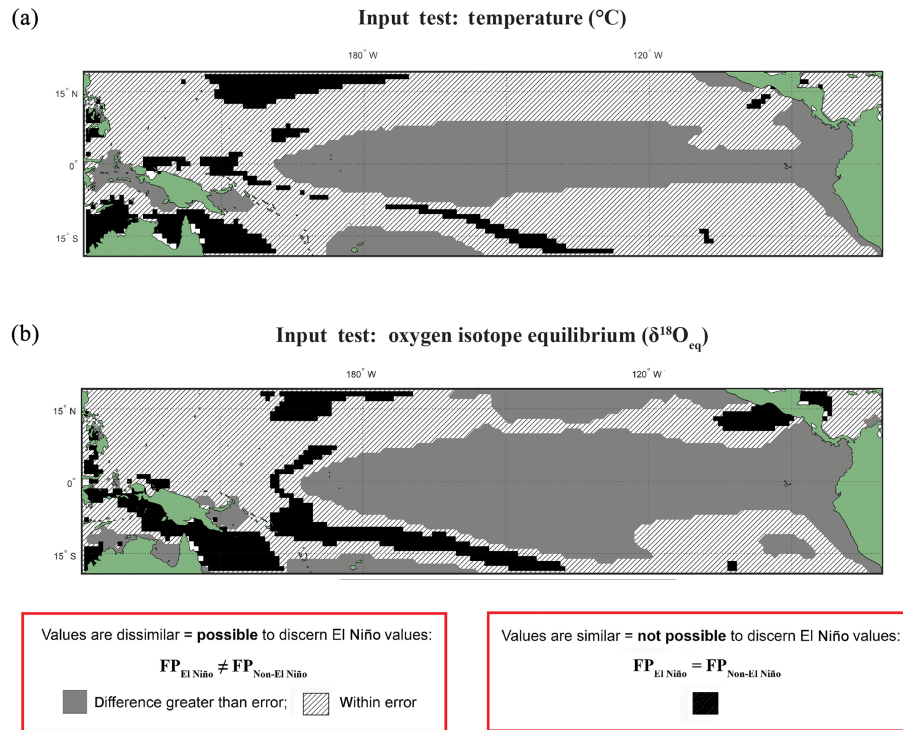


**Figure 1.** Anderson–Darling Results for input datasets of temperature and equilibrium  $\delta^{18}\text{O}$  ( $\delta^{18}\text{O}_{\text{eq}}$ ). Results of the test in which input variables underwent the same statistical procedure (see Sect. 2) as the modelled data for (a) temperature and (b)  $\delta^{18}\text{O}_{\text{eq}}$  values. Here, model input data were extracted for a single depth of  $\sim 5$  m without any growth weighting applied. Black regions are those grid points in which the null hypothesis ( $H_0$ ), that the El Niño and non-El Niño (neutral) foraminifera populations (FPs) are not statistically different ( $\text{FP}_{\text{El Niño}} = \text{FP}_{\text{Non-El Niño}}$ ), cannot be rejected. Grey regions represent grid points where the  $H_1$  hypothesis is accepted; therefore the distributions of the foraminiferal population for El Niño and non-El Niño can be said to be unique ( $\text{FP}_{\text{El Niño}} \neq \text{FP}_{\text{Non-El Niño}}$ ). The hatched regions represent areas where the  $H_1$  hypothesis can be accepted; therefore the distributions of the foraminiferal population for El Niño and non-El Niño can be said to be unique ( $\text{FP}_{\text{El Niño}} \neq \text{FP}_{\text{Non-El Niño}}$ ), though the difference between the means of tested distribution are less than (a)  $0.5^\circ\text{C}$  or (b)  $0.1\text{‰}$ . For a comparison with three different fixed depths (5, 149, and 235 m) without any growth weighting applied see Fig. S2.

al., 2009, 2011). This growth rate is then used as a weight to produce a growth-rate-weighted proxy value (Roche et al., 2018). The original Lombard et al. (2009, 2011) equations are based upon a synthesis of culture studies, pooled together irrespective of experimental design or rationale; therefore they can be considered to conceptually represent the fundamental niche of a given foraminiferal species, i.e. the range in environment that the species can survive. The basic structure of FAME is based upon temperature-based Michaelis–Menton kinetics to predict growth rate, described in Lombard et al. (2009), without using the parameters (e.g. light, respiration, and food) associated with FORAMCLIM (Lombard et al., 2011). The absence of known values or proxy values for the full set of parameters associated with FORAMCLIM has led us to seek a simplified approach in model parameterisation for FAME (Roche et al., 2018). It is important to note that through reducing the complexity of the problem of modelling foraminifera may lead to some deviation between observed and expected values. Our model assumes that temperature provides the dominant signal to the growth of

foraminifera, and therefore our results should be seen considering this assumption. Other processes may impact species growth such as mixed layer depth and nutrients.

#### 4.2.2 FAME species selection

Using the MARGO core top  $\delta^{18}\text{O}_c$  database (Waelbroeck et al., 2005), Roche et al. (2018) validated and computed the optimum depth habitat (the depth habitat that exhibits the strongest correlation when comparing FAME  $\delta^{18}\text{O}_c$  and MARGO  $\delta^{18}\text{O}_c$ ) for each species in the MARGO database. Whilst FAME can compute the growth rate of eight foraminiferal species from culture studies (Lombard et al., 2009, 2011; Roche et al., 2018), the limited number of species available for a global core top comparison necessitated a reduction in the number of species modelled (Roche et al., 2018). Here the output of FAME is further restricted to three species that have been the main focus of foraminifera-based studies that have been used to infer ENSO variability, namely the upper-ocean-dwelling *Globigerinoides sacculifer* and *Globigerinoides ruber*, as well

as the thermocline-dwelling *Neogloboquadrina dutertrei* (Ford et al., 2015; Koutavas et al., 2006; Koutavas and Joanides, 2012; Koutavas and Lynch-Stieglitz, 2003; Leduc et al., 2009; Sadekov et al., 2013). We use the  $1\sigma$  values of the observed (MARGO) minus expected (FAME), as computed by Roche et al. (2018) with the MARGO core top  $\delta^{18}\text{O}_c$  database, as the potential error associated with the FAME model. The MARGO database does not include *N. dutertrei* therefore it is not possible to estimate the FAME–MARGO error as can be done with *G. ruber* and *G. sacculifer* (Roche et al., 2018).

#### 4.2.3 FAME computation

ORAS4 temperature was used as the input variable (see Sect. 2), with the growth rate computations artificially constrained to the upper 60, 100, and 200 m to reflect the presence of photosymbiotic algae in the various foraminiferal species and an extreme value of 400 m. The modelled growth rate was used to compute the monthly depth-weighted oxygen isotope distribution for each species, using the aforementioned computed  $\delta^{18}\text{O}_{\text{eq}}$  for a given latitudinal and longitudinal grid point (Fig. 3). No correction for species-specific disequilibria, such as vital effect, was applied to the  $\delta^{18}\text{O}_{\text{eq}}$  values.

#### 4.2.4 Similar or dissimilar populations

A comparison, for each species, of FAME's predicted growth-weighted  $\delta^{18}\text{O}_c$  and  $T_c$  distributions associated with each climate event was done using an Anderson–Darling (AD) test. This statistical test can be used to determine whether or not two distributions can be said to come from the same population. The results of this test are presented in the following way: areas where the population distributions of the two climate states are found to be statistically similar have black grid cells in all panels referring to the Anderson–Darling test results (Figs. 2, S4–S6), and areas where the populations distributions of two climate states are found to be statistically distinct are shown in white. For plots including the potential error see Figs. S4 and S5. Where the Anderson–Darling test results of multiple species have been overlain the resultant plots represent where at least one species has dissimilar values (Fig. 2).

### 4.3 Results

Our results show that much of the Pacific Ocean can be considered to have statistically different populations between  $\text{FP}_{\text{EN}}$  and  $\text{FP}_{\text{NEU}}$  for both  $\delta^{18}\text{O}$  and  $T_c$  (Fig. 2). We consider that the likely cause for such a remarkable result is due to FAME computing a weighted average, and therefore, the lack of a signal found exclusively within the regions demarked in Fig. 1 as El Niño regions could represent how the temperature signal is integrated via an extension of the growth rate,

growing season, and depth habitat of distinct foraminiferal populations. Taking into account the FAME- $\delta^{18}\text{O}_c$  error for *G. ruber* and *G. sacculifer*, we have additionally computed regions in which the difference in oxygen isotopes between the two populations is smaller than the aforementioned error (see Sect. 4.2.2) (Hatching in Fig. S4), i.e. where the mean difference between  $\text{FP}_{\text{EN}}$  and  $\text{FP}_{\text{NEU}}$  is within the error. The hatched regions in Fig. S4 considerably reduce the areal extent of significant difference between  $\text{FP}_{\text{EN}}$  and  $\text{FP}_{\text{NEU}}$ , with the remaining regions aligning with the El Niño 3.4 region (Fig. S1). It is important to note that this error relates to the model, and in reality, the difference between the climate states could be larger or smaller. No such test was performed on the *N. dutertrei* dataset, because of its absence from the MARGO dataset. To further test the model-driven results and to assess if they are still consistent when the depth limitation is varied, the analysis was rerun with depths of 100, 200, and an extreme value of 400 m (Figs. S4–S6). Whilst it is possible to discern differences between the depths, it is important to note that a large percentage of the tropical Pacific remains accessible to palaeoclimate studies. A shallower depth limitation in the model increases the area for the “warm” species, suggesting that the influence of a reduced variability in temperature or  $\delta^{18}\text{O}_{\text{eq}}$  with a deeper depth limit causes the differences between  $\text{FP}_{\text{EN}}$  and  $\text{FP}_{\text{NEU}}$  to be reduced. Overlaying the results of the Anderson–Darling test for all three species (Figs. 2; S4–S6) per depth for 60, 100, and 200 m highlights the areas where multispecies comparisons could be made. To account for potential differences in depth habitat we make a combination of shallower depth for *G. ruber* and deeper depths for *G. sacculifer* and *N. dutertrei* (Pracht et al., 2019) in the final panels (Fig. 2b and d).

### 4.4 Discussion

A number of models and modelling studies exist to determine the foraminiferal responses to present (Fraile et al., 2008, 2009; Kageyama et al., 2013; Kretschmer et al., 2018; Lombard et al., 2009, 2011; Roy et al., 2015; Waterson et al., 2016; Žarić et al., 2005, 2006), past (Fraile et al., 2009; Kretschmer et al., 2016), and future (Roy et al., 2015) climate scenarios. Unlike some foraminiferal models, FAME does not include limiting factors such as competition, respiration, or predation variables, because no reliable proxy exists for such parameterisation in the geological record, and therefore aspects such as interspecific competition that may limit the niche width of a species are not computed. By identifying the optimum depth habitat, Roche et al. (2018) established the realised niche, i.e. the range in environment in which the species can be found, for these species for the Late Holocene. As these depth constraints ( $< 60$ ,  $< 100$ , and  $< 200$  m) may induce some variability we opted to include a conservative value of  $< 400$  m that grossly exaggerates the potential depth window. It is important to note, however, that as the computation of FAME is based on growth occurring within a temper-

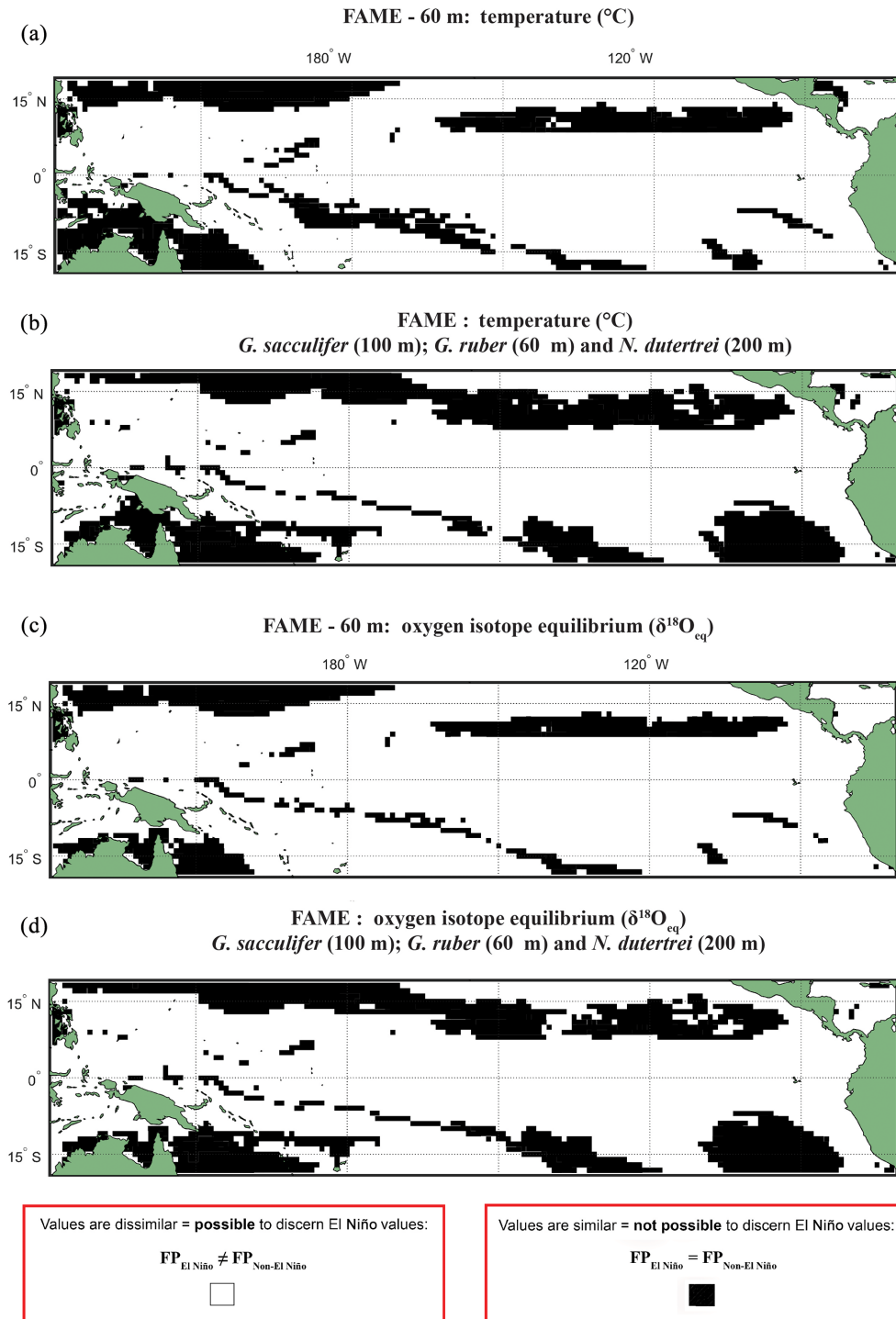


**Figure 2.** Anderson–Darling results plotted regionally in which species-specific results are overlain, for each plot the results represent where at least one species shows that it may not be possible to discern El Niño Values. Panels represent water depth locations where dissimilar and similar values for the two climate states for (a, b) FAME  $T_c$  modelled temperature and (c, d) FAME  $\delta^{18}\text{O}_c$  modelled oxygen isotope values recorded in the calcite shells ( $T_c$ ) occur. Each panel represents the Anderson–Darling test result. The results for *Globigerinoides sacculifer*, *Globigerinoides ruber*, and *N. dutertrei* are overlaid with (a, c) cut-off depth of 60 m and (b, d) species-specific cut-off values. For all panels, black areas reflect latitudinal and longitudinal grid points that failed to reject the null hypothesis ( $H_0$ ), and therefore the foraminiferal population (FP) of the El Niño is similar to the non-El Niño. Therefore the distribution between the neutral climate and El Niño cannot be said to be different ( $\text{FP}_{\text{El Niño}} = \text{FP}_{\text{Non-El Niño}}$ ).



ature window, it does not necessarily mean that for a given grid point modelled foraminifera will grow at depths down to 400 m (or whichever cut-off value is used), only that the model in theory can do so (depending if optimal temperature conditions are met). As the optimised depths computed from the MARGO dataset in Roche et al. (2018) are shallower, and upper ocean water is more prone to temperature variability, our approach likely dampens both the modelled  $\delta^{18}\text{O}_c$  and  $T_c$ . Indeed, the plots testing the input dataset (Sect. 3; Fig. 1) show that our FAME data, in which we allow the possibility for foraminiferal growth down deeper than the depths used in Roche et al. (2018), are a conservative estimate.

### 5 Experiment 3: FAME variance statistics

In Experiment 3 we examine the variance in the  $\delta^{18}\text{O}_c$  signal outputted by FAME for *G. sacculifer*. A fundamental problem with proxy records through sampling (Dolman and Laepple, 2018; Pisias and Mix, 1988; Wunsch, 2000; Wunsch and Gunn, 2003) is that they can be confounded by local regional climate and/or ENSO teleconnections that mimic ENSO changes, albeit at a different temporal frequency. The results of our Anderson–Darling testing may be unduly influenced by the Pacific decadal variability (PDV), also referred to as the Pacific Decadal Oscillation (PDO) (Pena et al., 2008). In much of the tropical Pacific the ratio of decadal to interannual  $\sigma\text{SST}$  suggests that they are comparable in magnitude; therefore fluctuations in SST are more obviously apparent outside of the purely canonical regions of ENSO (Wang et al., 2017). It could be that the areas outside of these canonical ENSO regions (Fig. S1) reflect the PDO (Pena et al., 2008; Wang et al., 2017). The study of ENSO has also focused on whether the variability is entirely in response to ENSO or whether it is dominated by interannual variability (Xie, 1994, 1995; Wang, 1994; Thirumalai et al., 2013). Therefore, in order to investigate how the signal may respond to a dynamic depth habitat, variance in the climate time series at each grid point was computed. As foraminiferal based ENSO studies have used the spread of the individual foraminifera isotope data (either standard deviation  $\sigma(\delta^{18}\text{O}_c)$  or its variance) as a measure of the increased variation in SST and, in turn, increased ENSO incidence and/or magnitude (Leduc et al., 2009; Zhu et al., 2017), this gives us the opportunity to compare our results. For each grid point both the total variance and the interannual variance,  $\sigma^2(\delta^{18}\text{O}_c)$ , of the FAME time series were computed in order to compare our results with previous studies. For the interannual variance, the computation follows the procedure outlined in Zhu et al. (2017). The mean monthly climatology is subtracted from the dataset, producing monthly anomalies and a linear trend removed (using the detrend function of MATLAB) – the resultant data was left unfiltered (i.e. Zhu et al., 2017 used a 1–2–1 filter). Comparison between the observed variance in FAME and expected data (Table 1) was done using the near-

est grid-cell. However, as foraminifera may drift during their life (van Sebille et al., 2015) a comparison was made with the average variance in a  $3 \times 3$  grid that has the nearest grid-cell to the core location at its centre. A comparison is also made with published iCESM model output for the same core locations (Zhu et al., 2017).

In a previous study, a Late Holocene sample ( $\sim 1.5$  ka) MD02-2529 ( $08^\circ 12.33' \text{ N}$ ,  $84^\circ 07.32' \text{ W}$ ; 1619 m) of *N. dutertrei* individual foraminifera ( $> 250 \mu\text{m}$  fraction) (Leduc et al., 2009) gave a  $\delta^{18}\text{O}$  standard deviation of 0.38‰. Here, the full  $\sim 60$ -year time series ( $n = 696$ ) of FAME gives a standard deviation for all species of between 0.26‰ and 0.32‰ ( $< 60$  m depth), between 0.20‰ and 0.29‰ ( $< 100$  m depth), between 0.20‰ and 0.25‰ ( $< 200$  m depth), and between 0.20‰ and 0.24‰ ( $< 400$  m depth) (see Table 1). However, these values can vary if the average of the surrounding grid cells is used (see Table 1). In comparison, the iCESM results have the following standard deviation values: for a Eulerian (fixed) depth of 50 m: 0.4‰; Eulerian depth of 100 m: 0.6‰; and Lagrangian: 0.49‰. There are three previously analysed samples (Koutavas and Joanides, 2012; Sadekov et al., 2013) located south of core site MD02-2529; these are the Late Holocene ( $\sim 1.6$  ka) samples of V21-30 ( $01^\circ 13' \text{ S}$ ,  $89^\circ 41' \text{ W}$ ; 617 m) and ( $\sim 1.1$  ka) V21-29 ( $01^\circ 03' \text{ S}$ ,  $89^\circ 21' \text{ W}$ ; 712 m) in which *G. ruber* was measured individually. For these two sites, the measured standard deviation is 0.507‰ and 0.510‰ for V21-30 and V21-29 respectively (Koutavas and Joanides, 2012). The third core site at a similar location is ( $\sim 1.6$  ka) CD38-17P ( $01^\circ 36' 04'' \text{ S}$ ,  $90^\circ 25' 32'' \text{ W}$ ; 2580 m) was not analysed individually. Instead replicates of pooled samples of two or three shells of *N. dutertrei* (Sadekov et al., 2013) were made, and these measured values give a standard deviation of 0.28‰. The full  $\sim 60$ -year time series ( $n = 696$ ) of FAME presented here gives a standard deviation for all species of between 0.33 and 0.41‰ ( $< 60$  m depth), between 0.27‰ and 0.40‰ ( $< 100$  m depth), between 0.25‰ and 0.35‰ ( $< 200$  m depth), and between 0.25‰ and 0.34‰ ( $< 400$  m depth) (see Table 1). Once again, these values can vary if the average of the surrounding grid cells is used (see Table 1). In comparison, the iCESM results have the following standard deviation values: for a Eulerian (fixed) depth of 50 m: 0.53‰; Eulerian depth of 100 m: 0.75‰; and Lagrangian: 0.35‰.

The use of the variance  $\sigma^2(\delta^{18}\text{O}_c)$ , or standard deviation  $\sigma(\delta^{18}\text{O}_c)$ , as an indicator of ENSO is dependent on whether the variance in the original climate signal was dominated by interannual variance. Zhu et al. (2017) computed the total variance change with and without the annual cycle, suggesting that for some cores the increased assumed ENSO variability at the LGM as deduced by proxy records (Koutavas et al., 2006; Koutavas and Joanides, 2012; Koutavas and Lynch-Stieglitz, 2003) may be purely a byproduct of the annual cycle or dominated by it. Computing the ratio between the interannual (Fig. 3c) and total variance (Fig. 3a) of FAME

**Table 1.** Data–model comparison.

Genus	Species	Model iteration cut-off depth (in m)	Total standard deviation (in %)			Interannual standard deviation (in %)			Ratio between total and interannual	Data reference (in %)	Data (age in kyr)	iCESM model Eulerian view (50 m); standard deviation in %	iCESM model Eulerian view; standard deviation in %	iCESM Lagrangian view; standard deviation in %
			Closest grid cell value	Mean of 3 × 3 grid	Range of 3 × 3 grid	Closest grid cell value	Mean of 3 × 3 grid	Range of 3 × 3 grid						
<i>Globigerinoides</i>	<i>sacculifer</i>	60	0.32	0.33	0.03	0.29	0.29	0.05	0.90	0.89	0.10	0.40	0.60	0.49
		60	0.38	0.42	0.16	0.31	0.33	0.09	0.82	0.79	0.17	0.53	0.75	0.35
	<i>ruber</i>	60	0.26	0.27	0.01	0.23	0.23	0.03	0.88	0.88	0.13	0.40	0.60	0.49
		60	0.33	0.37	0.13	0.26	0.27	0.08	0.79	0.75	0.20	0.53	0.75	0.35
	<i>Neogloboquadrina dutertrei</i>	60	0.32	0.32	0.06	0.26	0.26	0.02	0.79	0.82	0.17	0.40	0.60	0.49
		60	0.41	0.45	0.18	0.33	0.35	0.11	0.81	0.78	0.16	0.53	0.75	0.35
<i>Globigerinoides</i>	<i>sacculifer</i>	100	0.25	0.26	0.03	0.22	0.22	0.04	0.88	0.87	0.12	0.40	0.60	0.49
		100	0.33	0.36	0.14	0.28	0.29	0.08	0.84	0.81	0.16	0.53	0.75	0.35
	<i>ruber</i>	100	0.20	0.21	0.07	0.16	0.16	0.02	0.80	0.80	0.23	0.40	0.60	0.49
		100	0.27	0.31	0.11	0.22	0.22	0.08	0.79	0.73	0.23	0.53	0.75	0.35
	<i>Neogloboquadrina dutertrei</i>	100	0.29	0.29	0.05	0.23	0.23	0.02	0.79	0.82	0.17	0.40	0.60	0.49
		100	0.40	0.43	0.15	0.33	0.34	0.09	0.83	0.81	0.11	0.53	0.75	0.35
<i>Globigerinoides</i>	<i>sacculifer</i>	200	0.21	0.22	0.04	0.17	0.18	0.02	0.83	0.81	0.20	0.40	0.60	0.49
		200	0.28	0.31	0.11	0.23	0.25	0.09	0.83	0.78	0.21	0.53	0.75	0.35
	<i>ruber</i>	200	0.20	0.20	0.09	0.16	0.16	0.03	0.78	0.79	0.24	0.40	0.60	0.49
		200	0.25	0.29	0.10	0.18	0.20	0.07	0.74	0.69	0.27	0.53	0.75	0.35
	<i>Neogloboquadrina dutertrei</i>	200	0.25	0.25	0.05	0.20	0.20	0.02	0.78	0.81	0.16	0.40	0.60	0.49
		200	0.35	0.37	0.11	0.30	0.31	0.08	0.85	0.83	0.10	0.53	0.75	0.35
<i>Globigerinoides</i>	<i>sacculifer</i>	400	0.21	0.22	0.04	0.17	0.18	0.02	0.83	0.81	0.20	0.40	0.60	0.49
		400	0.28	0.31	0.11	0.23	0.24	0.09	0.83	0.78	0.21	0.53	0.75	0.35
	<i>ruber</i>	400	0.20	0.20	0.09	0.16	0.16	0.03	0.78	0.79	0.24	0.40	0.60	0.49
		400	0.25	0.29	0.10	0.18	0.20	0.07	0.74	0.69	0.27	0.53	0.75	0.35
	<i>Neogloboquadrina dutertrei</i>	400	0.24	0.23	0.05	0.18	0.19	0.02	0.77	0.80	0.17	0.40	0.60	0.49
		400	0.34	0.36	0.11	0.29	0.30	0.07	0.85	0.83	0.10	0.53	0.75	0.35

Data from the following sources: <sup>a</sup> Leduc et al. (2009), <sup>b</sup> Koutavas and Joannides (2012), and <sup>c</sup> Sadekov et al. (2013). Model (iCESM) values from supplement of Zhu et al. (2017) (converted from variance).

(Fig. 3b; see Table 1), our results have a similarly high ratio of interannual to total variance as iCESM and SODA reanalysis (Carton et al., 2000a, b; Zhu et al., 2017). Even in regions in the eastern equatorial Pacific (EEP) wherein the ratio reduces, it is still above  $> 0.5$ . Although the values of El Niño can be considered significantly different from other climate states (Sect. 4), our own analysis using the ratio of total to interannual variance also suggests that much of the variance in the simulated foraminiferal signal is dominated by interannual variance. There are differences in the ratio of total to interannual variance between species and in different regions of the tropical Pacific; however, even with a dynamic depth habitat this ratio is still high (Fig. 3; Table 1).

## 6 Experiment 4: FAME picking experiment

### 6.1 Objective

In Experiment 4 we perform a series of picking experiments on our FAME output. One source of potential variation in palaeoceanographic analysis is related to the necessity of picking a finite sample for geochemical analysis, with the intention being that the picked sample is a robust estimate of the population average without necessarily measuring every individual that constitutes a population. Picking can generate a series of biases within reconstructions. For instance, picking could technically bias the result if instead of a uniform distribution a particular event/seasonal/depth-habitat produces a larger flux of individuals, thereby over-emphasising one aspect of the environment to the detriment of others. Several “picking” experiments were performed to determine the variance between picking iterations; the focus here has been related to comparison between grid points and the potential machine error or depth habitat.

### 6.2 Methodology

As FAME is not an individual foraminiferal analysis model, it instead computes the average value for a given time step (i.e. here it is the average of a single month). Therefore with respect to terminology what we are in effect picking is individual months rather than individual specimens. Kept constant between each experiment were the following: the number of months drawn ( $n = 60$ ), that each month was drawn with replacement, and that the number of Monte Carlo iterations is set at 10 000. No attempt to parameterise for misidentification has been done, as although one could assign a random value to a small percentage of the modelled values (conceptually one can argue that misidentification assigns an incorrect value), the assigned value would require knowledge of the values of co-occurring species. Previous work has highlighted the range in and between co-occurring specimens from different species (e.g. Feldmeijer et al., 2015; Metcalfe et al., 2015, 2019a). Therefore, the assumption is made that the “picker” is taxonomically well-trained and/or has a pro-

cedure in which species can be checked taxonomically post-analysis, e.g. photographing all specimens prior to analysis (e.g. Pracht et al., 2019).

For Picking Experiment I (Fig. 4a) all grid points have the same selected months per iteration of Monte Carlo; i.e. there are  $10\,000 \times 60$  selected months. This assumes that the picker picks the same months at hypothetical grid point A as they select at grid point B. In Picking Experiment II (Fig. 4b), a grid-point-specific individual Monte Carlo was run; i.e. there are  $170 \times 40 \times 10\,000 \times 60$  selected months. This assumes that different months could be selected between hypothetical grid point A and point B. In Picking Experiment III (Fig. 4c), at each grid point a Monte Carlo was run using the growth rate weighting for each month (i.e. there are  $170 \times 40 \times 10\,000 \times 60$  selected months). This assumes that in periods of higher growth there will be a higher flux of the species and therefore a greater chance of selecting that month. The rationale being that researchers will not pick specimens representing identical time periods between grid point A and point B. In Picking Experiment IV (Fig. 4d and 4e), the second experiment was rerun but with the addition of two sources of error; the first error is based upon FAME producing the average value for a given time slice; therefore short-term variability in temperature and/or the spread in the population (i.e. variance in depth of an individual; variance in chamber growth per individual), as evidenced by single-foraminiferal analysis of sediment trap samples (e.g. Steinhart et al., 2015), is potentially lost. For each picked month we therefore randomly added between  $-0.40\text{‰}$  and  $+0.40\text{‰}$  (approximately  $\pm 2\text{°C}$ , i.e. for a full range of  $\sim 4\text{°C}$ ) to its value in intervals of  $0.02\text{‰}$ . The second error is the analytical error that an individual measurement will have. Machine measurement error is assumed to lie between  $-0.12\text{‰}$  and  $0.12\text{‰}$  (in intervals of  $0.005\text{‰}$  – the third decimal place is an exaggeration of machine capabilities, although it will have repercussions for rounding), the  $1\sigma$  of within-run average (as opposed to long-term average) of international stable isotope standards. The intervals of both errors ( $0.02\text{‰}$  and  $0.005\text{‰}$ ) were chosen to give a similar number ( $n = 41$  and  $49$ ) of potential randomly selected error for each picked month. For this experiment the value assigned to each picked month was a (grid-point-specific) randomly selected value for both of these errors. The values for within-month variability (Fig. 4d) and machine error (Fig. 4e) are calculated separately and then combined (Fig. 4f), as they may have a corresponding or conflicting sign, either “cancelling” out each other or amplifying the difference.

### 6.3 Result

The Monte Carlo experiments (Fig. 4a–f) highlight the variation in picking a subset of the months, here 60, from the full time series. Given the complexity in reconstructions of trace metal geochemistry (Elderfield and Ganssen, 2000; Nürnberg et al., 1996) the focus of the picking here has been on

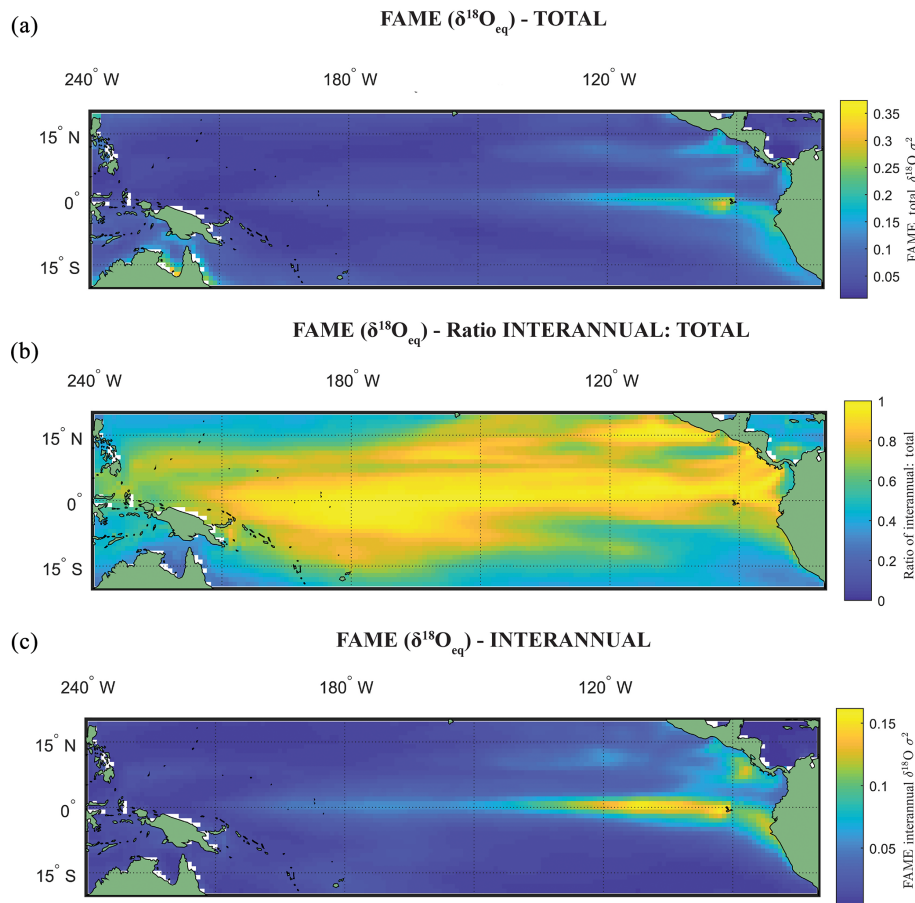


**Figure 3.** Total variance and interannual variance. **(a)** Total variance in *Globigerinoides sacculifer*  $\delta^{18}\text{O}_c$ , using FAME  $\delta^{18}\text{O}_{\text{eq}}$  for a cut-off value of 60 m. **(b)** The ratio of **(a)** and **(c)**, where **(c)** is the interannual variance in the time series of **(a)**.

the  $\delta^{18}\text{O}_c$ . The FAME- $\delta^{18}\text{O}_{\text{eq}}$  *G. sacculifer* with a depth cut-off of 60 m is plotted here. The values for each grid point is the range in standard deviation (i.e. the maximum standard deviation minus the minimum standard deviation) between iterations of Monte Carlo ( $n = 10000$ ). The range in standard deviations between iterations is plotted instead of the mean of the standard deviations; with increasing  $n$  the mean converges toward the sample mean. However as the point of Monte Carlo is to generate plausible samples, it is more important to take into account the range in possible values which would help to establish the potential variability of subsampling. For the most part, regions with high total variance (Fig. 4a) also have a larger range in standard deviations between the iterations picked. It is interesting to note that by changing from the same months picked for each grid point (Monte Carlo I, Fig. 4a) to varying the months picked between grid points (Monte Carlo II, Fig. 4b or Monte Carlo III, Fig. 4c) the range goes from smooth to a more noisy dataset. Whilst the values plotted here are not the absolute values (as they are the range in standard deviation for a given grid point for the entire 10 000 iterations), it can be seen that some of the inter-core comparisons could in essence relate to

differences in picking; i.e. different months picked between grid points may exacerbate or accentuate differences. Likewise, adding random variability, between  $-0.4\text{‰}$  and  $0.4\text{‰}$  (Fig. 4d and f), may also reduce the differences between areas of high total variance and low total variance. The values associated with machine error ( $-0.12\text{‰}$  to  $0.12\text{‰}$ ), however, appear to do little to affect the range (Fig. 4e and f). Whilst again the values plotted are not the absolute values, the variability added in an attempt to mimic biological variation of a given time slice increases the range of possible standard deviations in regions with low total variance (Fig. 4d and e). Therefore, understanding the biological variability on shorter timescale (e.g. Steinhardt et al., 2015; Mikis et al., 2019), which maybe here over-exaggerated, may be crucial for understanding discrepancies between cores.

## 7 Experiment 5: approximation of sediment archives

### 7.1 Objective

In Experiment 5 we compare our FAME results with bathymetric and sedimentological features of the tropical Pacific.

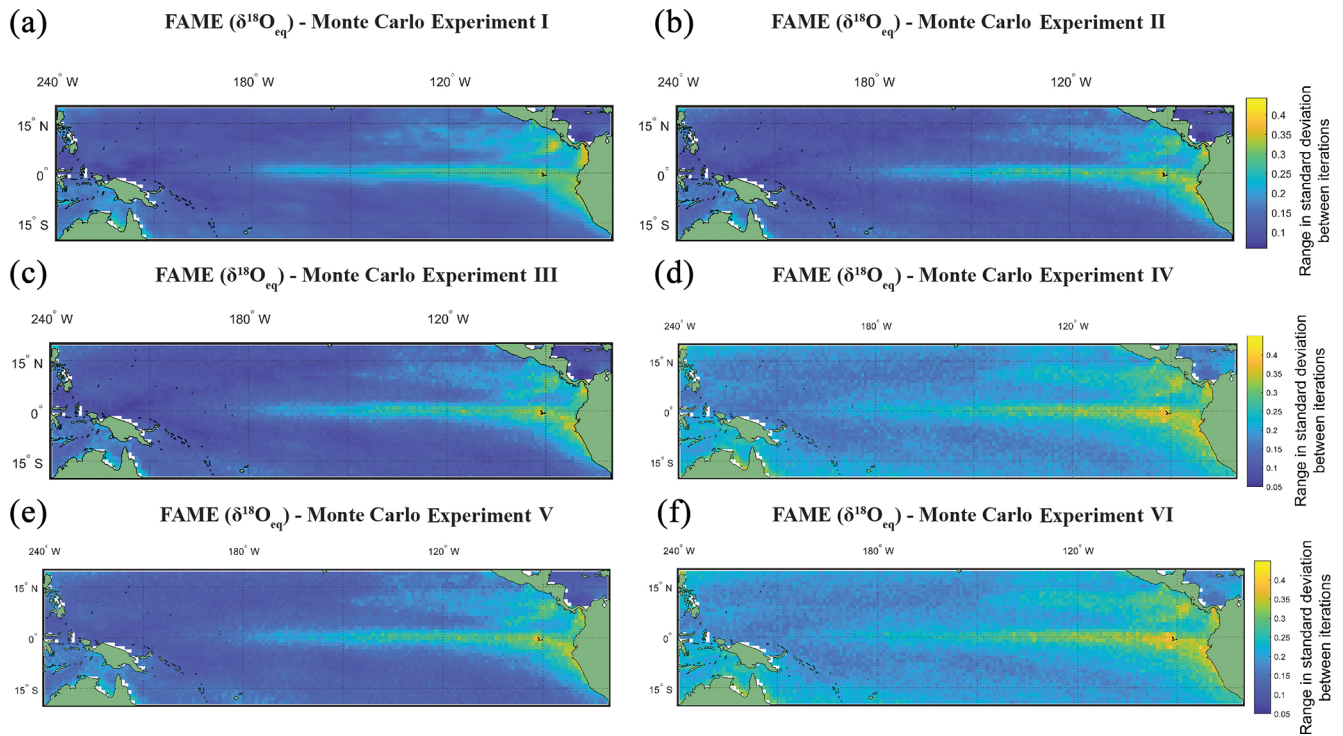


**Figure 4.** The range in standard deviation of the Monte Carlo experiments using FAME- $\delta^{18}\text{O}_c$  *G. sacculifer* with a depth cut-off of 60 m. In (a)–(f) we plot the range in standard deviation obtained by picking 60 months with replacement with 10 000 iterations. The experiments are as follows: (a) the same months were chosen for all grid points for each iteration of Monte Carlo; (b) each grid point has its own randomly selected months for each iteration of Monte Carlo; (c) the same as (b), but we weight the values by the total amount of growth per month; (d) the months selected for (c) were rerun, but a random variability is added to each month (between  $-0.4\text{‰}$  and  $0.4\text{‰}$ ); (e) the months selected for (b) were rerun, but a random measurement error is added to each month (between  $-0.12\text{‰}$  and  $0.12\text{‰}$ ); and (f) the months selected for (b) were rerun, but the (d) random variability and (e) measurement error were combined.

The preceding analysis has focused upon  $\sim 60$ -year reanalysis data. Such a comparable resolution would require a core to have a similar temporal resolution of  $\sim 60$  years. The hypothetical core should also be above the lysocline to allow for the recovery of a proxy signal equivalent to the original climate signal. At lower sedimentation rates the modification of the original ambient climate signal is not limited to just its translation into a foraminiferal proxy signal and the shift in position of sinking foraminifera (van Sebille et al., 2015; Deuser et al., 1981), but rather it can also be affected by the dissolution of calcium carbonate in the water (Schiebel et al., 2007), at the seafloor, or due to pore fluids and bioturbation. Much of the deep-sea Pacific is both below the lysocline and has a sediment accumulation rate (SAR) that is very low (e.g. Hays et al., 1969 at  $0.96 \pm 0.43 \text{ cm kyr}^{-1}$ ), although there are regions that satisfy both bathymetry and enhanced sedimentation (e.g. Koutavas and Lynch-Stieglitz, 2003 at  $7.20 \pm 2.82 \text{ cm kyr}^{-1}$ ). In the following section we investigate where in the tropical Pacific it is possible to extract environmental information with short frequencies from foraminiferal-based proxies. We consider that a core site must be largely unaffected by dissolution (i.e. above the lysocline) so as not to adversely affect the foraminifer population,

and the sedimentation rate must be high enough to minimise, as much as possible, the disturbance of the downcore temporal record by bioturbation.

## 7.2 Methodology

### 7.2.1 Dissolution: cut-off depth rationale

Whilst the presence of water depths in the ocean lacking calcite-rich sediment was described in the earliest work (e.g. Murray and Renaud, 1891; Sverdrup et al., 1942), overlaying maps of measured surface sediment carbonate percentage with water depth in the Pacific Ocean led Bramlette (1961) to coin the term “compensation depth” (Wise, 1978). This work highlighted the “narrow” depths of the carbonate compensation depth (CCD) in the central Pacific (4–5000 m). Conceptually Berger (1971) placed three levels in the Pacific Ocean that were descriptive of the aspects (e.g. chemical, palaeontological, and sedimentological) of the calcite budget; the saturation depth, demarcating supersaturated from undersaturated; the lysocline, the depth at which dissolution becomes noticeable (Berger, 1968, 1971); and compensation depth (Bramlette, 1961), in which supply is compensated through dissolu-

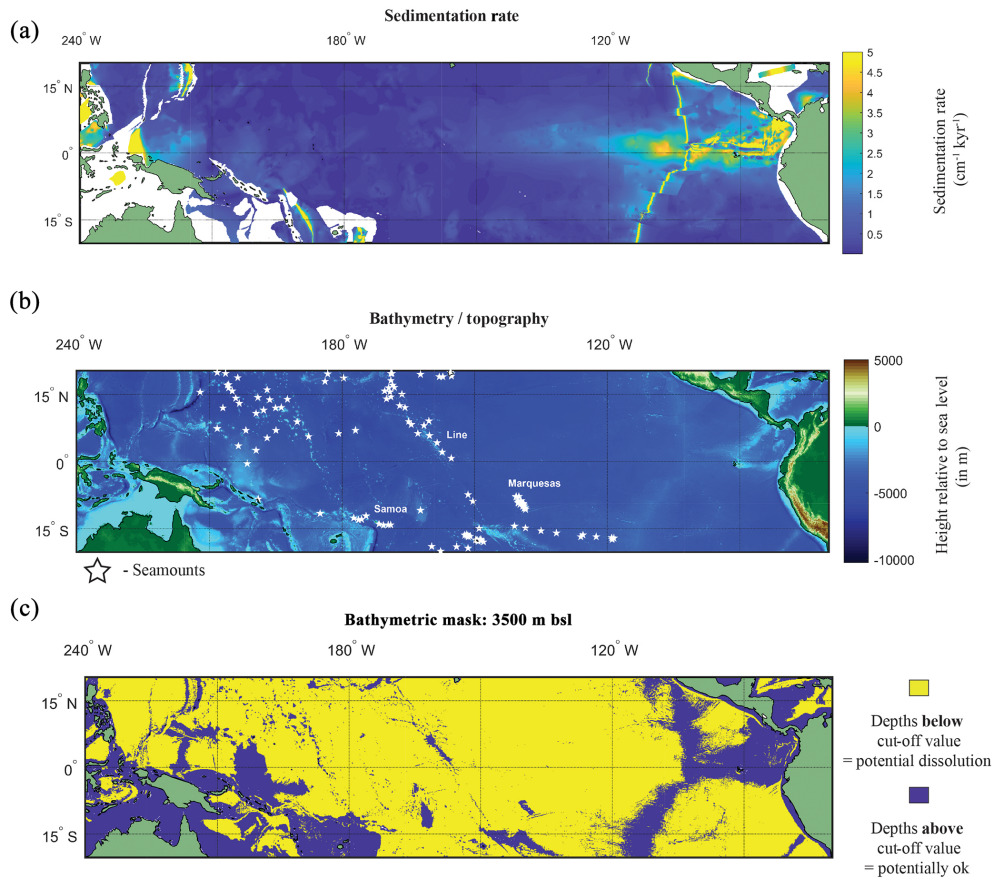


**Figure 5.** (a) Map of the sedimentation rate and bathymetry of the tropical Pacific. (a) Inferred sedimentation rate (Olson et al., 2016). White regions represent continental shelf. (b) GEBCO map of height relative to 0 m with location of seamounts plotted (white stars). (c) A binary colour map of the GEBCO data; yellow is values below cut-off depth value ( $> 3500$  m below sea level – b.s.l.), and purple is above the cut-off depth value. See Fig. S8 for variation in cut-off values.

tion. The lysocline and carbonate compensation depth (CCD) vary between the different ocean basins; the modern Atlantic Ocean in which deep water forms has a relatively deep CCD as a byproduct of being young, well-ventilated bottom waters whereas, the Pacific Ocean (the final portion of the global thermohaline circulation) has a shallower CCD.

### 7.2.2 Dissolution approximation

Dissolution is approximated by determining if each grid cell's corresponding depth value is above or below the prescribed cut-off value. For much of the equatorial Pacific the lysocline is estimated by a foraminiferal assemblage methodology at  $\sim 3800$  m (Parker and Berger, 1971). However as the lysocline is where dissolution becomes apparent (ergo it is a sample already visibly degraded), we first set the limit of the water depth mask shallower, at 3500 m b.s.l. In order to account for potential variability, two further depths were used as cut-off values: 4000 and 4500 m b.s.l. These depths represent multiple possible depths under which there is the potential for noticeable dissolution (i.e. lysocline) or com-

plete dissolution (i.e. CCD). The bathymetry of the Pacific was extracted from the General Bathymetric Chart of the Oceans (GEBCO) 2014 grid, in 30 arcsec intervals (version 20150318; <https://www.gebco.net/>, last access: 21 December 2017), between  $-20^\circ$  S to  $20^\circ$  N and  $120^\circ$  E to  $-70^\circ$  W (Fig. 5b). A compilation of seamounts was also plotted, as these bathymetric features may provide sufficient height to allow preservation of sediment alongside higher sediment accumulation rates (Batiza, 1982; Clouard and Bonneville, 2005; Hillier, 2007; Koppers et al., 2003; Menard, 1964; Wessel and Lyons, 1997).

### 7.2.3 Bioturbation

If we factor in the sedimentation rate of the Pacific, which in some regions has been estimated to be lower than  $1 \text{ cm ka}^{-1}$  (Blackman and Somayajulu, 1966; Hays et al., 1969; Menard, 1964), then dissolution may become further exacerbated. A secondary factor is bioturbation. Systematically bioturbated deep-sea sediment cores can produce discrete sediment intervals with foraminifera that have

ages spanning many centuries and/or millennia (Berger and Heath, 1968; Lougheed et al., 2018; Peng et al., 1979). In order to model the effect of bioturbation upon the age distribution of discrete core depths, a number of studies have used a diffusion-style approach that reduces the parameters down to SAR and sediment mixing depth (herein referred to as bioturbation depth, BD), although this may be an artificial division purely driven by mathematical need rather than biological constraints (Boudreau, 1998). The BD has been shown to have a global average of  $9.8 \pm 4.5$  cm ( $1\sigma$ ) that is independent of both water depth and sedimentation rate (Boudreau, 1998), likely controlled as a result of the energy efficiency of foraging (e.g. deeper burrows may cost more energy to produce than can be offset in extracted food resources) and potential decay in labile food resources with sediment depth.

Following the current available geochronological method (i.e. age–depth method) single specimens that are displaced in depth are assigned the average age of the depth to which they were displaced, which will result in erroneous interpretations of climate variability when analysis such as individual foraminiferal analysis (IFA) is applied (Lougheed et al., 2018). To investigate how much temporal signal is integrated into discrete-depth intervals for typical tropical Pacific SAR (Olson et al., 2016; adapted by Lougheed et al., 2018) the single-foraminifera SEDiment AccuMulation Simulator (SEAMUS; Lougheed, 2020b) was utilised to bioturbate a climate signal. As it is not possible to carry out a transient bioturbation model with the SAR and BD of the Pacific with only 0.5 century of data (such as the ORAS4 temperature and salinity ocean reanalysis data), a longer highly temporally resolved climate input signal was used to explore the effect of bioturbation upon a given climate signal. The 0–40 000-year  $\delta^{18}\text{O}_w$  of NGRIP (North Greenland Ice Core Project Members, 2004; Rasmussen et al., 2014; Seierstad et al., 2014) is considered to be a satisfactory replacement signal to simulate a foraminiferal signal in 10-year time steps. It must be stressed that the use of the NGRIP time series here is purely as an input parameter to investigate the effect of bioturbation upon an oxygen isotope-based climate signal. It is important to further stress that by using NGRIP as an input signal for SEAMUS we are implying neither that tropical Pacific cores should have a signal similar to NGRIP nor that we are translating the NGRIP signal to the tropical Pacific or inferring some kind of causal relationship. As we seek to investigate the effect of bioturbation, no attempt has been made to modulate the absolute values of the input signal to mimic expected  $\delta^{18}\text{O}_c$  values, and this is why each plot of the synthetic down core time series retains the use of V-SMOW, despite carbonates being required to be V-PDB (Coplen, 1995).

A single parameter was varied whilst all others were kept constant between experiments with SEAMUS. Values of SAR were varied to fixed values of 1, 2, 5, or 10 cm kyr<sup>-1</sup>, which are representative of typical Pacific SAR. As the oxygen saturation state of the Pacific Ocean bottom waters is above 40 % (Fig. S9), suggestive that oxygen may not be a

limiting factor, values of BD of 5, 10 or 15 cm were used. These values are based upon the global estimate of BD and its error bounds (Boudreau, 1998). For each experiment, the selected values of SAR and BD were kept constant for the entire SEAMUS model run (i.e. the intensity and magnitude of bioturbation was not varied), although in reality SAR and BD may vary temporally depending on local conditions. Each experiment was plotted as a histogram of the frequency of the age of specimens in the BD, where the BD represents different thicknesses of sediment (5, 10, and 15 cm), and a time series using the computed discrete 1 cm depth median age (Fig. 9).

### 7.3 Results and discussion

A factor in the postmortem preservation of the oceanographic signal in foraminiferal shells is whether the shells can be preserved. Irrespective of the bathymetric cut-off value used for the GEMCO bathymetry data, it is evident that much of the canonical El Niño 3.4 region used in oceanography, as well as a large proportion of the tropical Pacific, is excluded from suitability as a perspective core site (Fig. 5b and c). Even in regions where bathymetry may be above the cut-off value dissolution may occur. For instance, in regions of high fertility, such as the EEP, the lysocline was estimated to be present at  $\sim 2800$  m (Thunell et al., 1981) or  $\sim 3000$  m (Berger, 1971; Parker and Berger, 1971). In the EEP region the shallower lysocline is accompanied by an equally shallower CCD (located at  $\sim 3600$  m) for which the high fertility/primary production is considered responsible for its shoaling, lowering the pH through increased CO<sub>2</sub> (Berger et al., 1976). The correspondence between lysocline depth and CCD depth does not hold true for the entirety of the Pacific. Plotting a N–S cross section from 50° N to 50° S, Berger (1971) noted that in the central equatorial Pacific, the high-fertility region generates a larger zone of dissolution resistant facies even with a shoaled lysocline. A second factor is the sedimentation rate. Using a cut-off value that has been previously considered sufficiently high enough to outpace bioturbation (e.g. Koutavas and Lynch-Stieglitz, 2003) of 5 cm kyr<sup>-1</sup>, it can be demonstrated that much of the Pacific has an inferred lower sedimentation rate ( $< 5$  cm kyr<sup>-1</sup>; Fig. 5a).

Overlaying the water depth and the SAR with the Anderson–Darling results (Figs. 6 and S7) highlights that of the total area where FP<sub>EN</sub> is significantly different from FP<sub>NEU</sub> (i.e. those areas where planktonic foraminiferal flux is suitable for reconstructing past ENSO dynamics), only a small proportion corresponds to areas where the sea floor is both above the CCD ( $< 3500$  m b.s.l.) and SAR is at least 5 cm ka<sup>-1</sup> (Fig. 7). However, at certain locations, near islands or seamounts, the SAR and water depth may be high enough to allow for a signal to be preserved (Fig. 5b) that may not be represented here.

The results of the bioturbation simulator SEAMUS, plotted as a time series of the bioturbated NGRIP signal (Fig. 8)

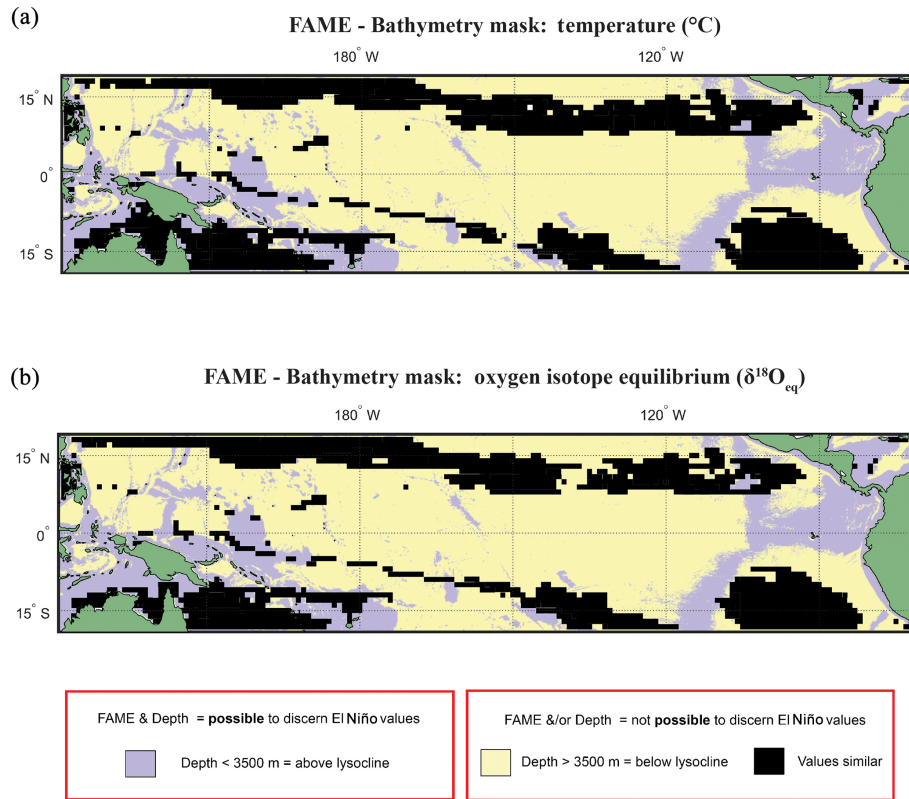


**Figure 6.** Overlay between bathymetry and FAME results. The results of the FAME Anderson–Darling test for (a) temperature and (b) oxygen isotope values as input. Locations where the  $H_1$  hypothesis can be accepted, i.e. where the distributions can be said to be different ( $FP_{ElNiño} \neq FP_{Non-ElNiño}$ ), are plotted as yellow where the depth is deeper than 3500 m b.s.l. or purple where the depth is shallower than 3500 m b.s.l. (see Fig. 2). Purple locations are where our results suggest that the signal of ENSO has different values and the water depth allows for preservation.

and as histograms of the probability of finding a particularly pseudo-foraminifera with a given age within the bioturbation depth (Fig. 9), highlight the potential single-foraminifera depth displacement that occurs with low sedimentation rates (Fig. 5). Within a single depth in a core, proxy values largely represent the integrated time signal for that depth. The age of specimens within the bioturbation depth may vary from a few to tens of thousands of years (Fig. 9). A data–model comparison without sufficient knowledge of bioturbation may equate an integrated proxy signal with a climatic signal for an inferred (or measured) average age for the depths in question. For proxies that use an average values (i.e. a pooled foraminiferal signal) or a variance (i.e. individual foraminifera values), the individuals will be based upon a nonuniform distribution in temporal frequency of specimens; i.e. older specimens are few compared to younger specimens. A large proportion of the specimens in the BD come from years that are “proximal” (i.e. close to the youngest age) which may give undue confidence that the probability of picking a specimen from these years is higher. However the long tail of the distribution means that there is an equally high chance of picking a specimen that has come from sev-

eral thousand years earlier than the median age of the discrete depth. Whilst the temporal integration involved in bioturbation can be problematic for either age–depth modelling (e.g. Lougheed et al., 2018) or discrete age measurements (e.g. Lougheed et al., 2020) it will also integrate the climate signal carried by the individual foraminifera.

If for example the spread in a climate variable, such as temperature, is uniform throughout the integrated time (and the abundance at each temperature value is also uniform), then it could be possible to reproduce a similar temperature distribution in bioturbated cores, although this would not by definition represent the actual spread in the actual climatic variable for a given time. However, the climate signal is unlikely to be constant, integrating a climatic signal bioturbation can therefore introduce artefacts inducing the possibility of spurious interpretations. Of course, identification of spurious datapoints are more obvious where the measured distributions over-exaggerate the climate signal (e.g. Wit et al., 2013). Our simulation of a climate signal reveals (Fig. 8) the following: a reduction in signal amplitude with low SAR and/or increasing BD, loss of short events at low SAR, a shift in the apparent timing of events with increasing BD, and an



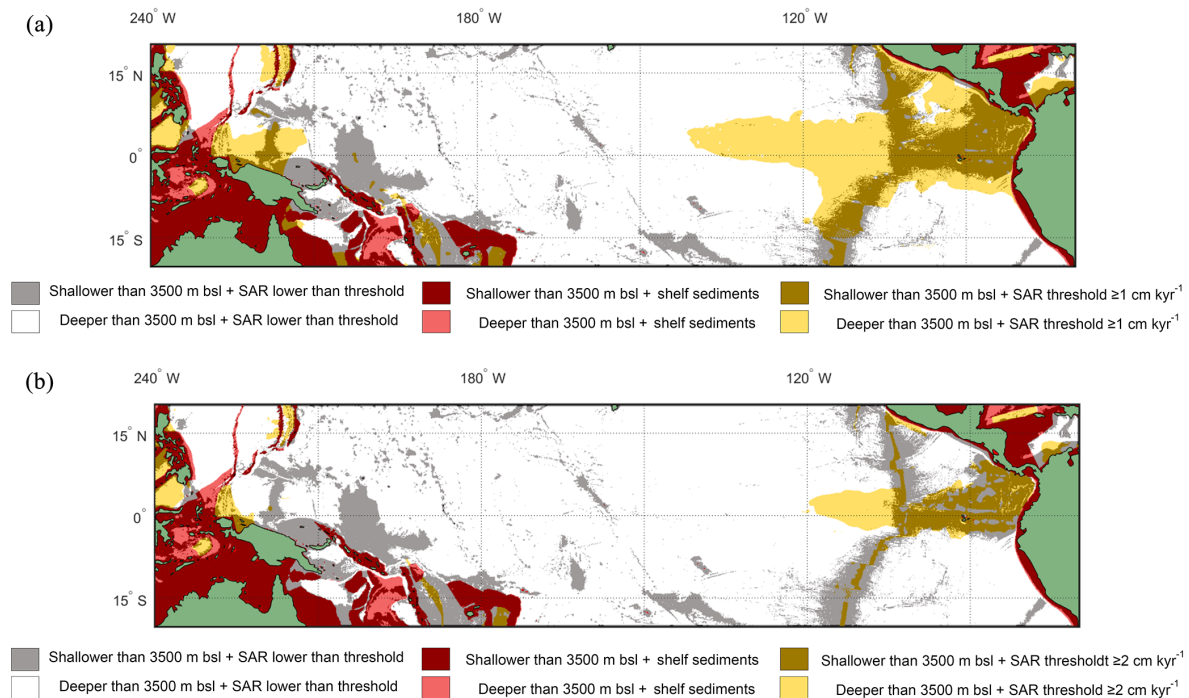


**Figure 7.** Overlay between water depth and inferred SAR (Olson et al., 2016). Cut-off limits for bathymetry and SAR are 3500 m below sea level and (a)  $\geq 1$  cm kyr<sup>-1</sup> and (b)  $\geq 2$  cm kyr<sup>-1</sup> respectively. The colours represent the following: red/pink: continental shelf sediments that are (red) shallower or (pink) deeper than 3500 m b.s.l.; grey/white: grid point SAR is lower than SAR threshold and the seafloor depth is (grey) shallower or (white) deeper than 3500 m b.s.l.; light yellow/gold: light yellow represents areas where the SAR is above the threshold, but the water depth is deeper than 3500 m b.s.l., while in comparison gold represents areas where the SAR is above the threshold and the water depth is shallower than 3500 m b.s.l. The ideal locations are therefore plotted as gold.

apparent increasing core-top age with low SAR and increasing BD (Fig. 9). The median age of the bioturbation depth (Fig. 9) is the reason why each time series (Fig. 8) does not “start” at an age of zero (Keigwin and Guilderson, 2009).

Whilst we are principally interested in understanding whether living foraminifera can theoretically reconstruct ENSO, the results of the sedimentological features, presented here, imply that much of the Pacific Ocean is not suitable for preserving (Figs. 5–9) the ENSO signal, despite the possibility of the species of foraminifera in the water having unique values for different climate states (Sect. 4; Fig. 6). In areas where preservation could occur, a hypothetical core could allow for the possible disentanglement of El Niño-related signals from the climatic signal but only in a best-case scenario involving minimal bioturbation, which is unlikely in the case of oxygenated waters. Combined with finite sampling strategies, the effects of both dissolution and bioturbation can be further amplified.

## 8 Discussion

### 8.1 Palaeoceanographic implications

Ecophysiological proxy system models are a mathematical approximation aimed at replicating the proxy signal both as

its response to and modification of the original target climate signal (e.g. Dee et al., 2015). Linking ecophysiological models to coupled ocean–atmosphere models (e.g. Clement et al., 1999; Zebiak and Cane, 1987), isotope enabled Earth system models (e.g. iCESM; Zhu et al., 2017) or multimodel ensembles with prescribed boundary conditions could be used for the generation of time series for testing presumptions in proxy studies. Used a priori, an explicit forward model can be implemented to test if it is plausible that the given recording system can record an oceanographic signal to allow robust reconstructions.

A critical presumption in proxy studies is embedded in site selection. Sites selected are presumed to be able to (or not) generate a climate signal. The presumptive answer in such studies is either the feature occurs or did not occur, and if it occurs then it has either enhanced or weakened. Such a presumption precludes a scenario in which the feature or oceanographic regime has shifted, passing over or beyond a core site (Weyl, 1978), reacting to the expansion, contraction, or shift of certain large-scale oceanographic features (e.g. polar front, upwelling) during periods of either warmer than average (e.g. the last interglacial) or colder than average temperatures (e.g. glacial maxima). The analysis of recent El Niño patterns suggests that there are two types of

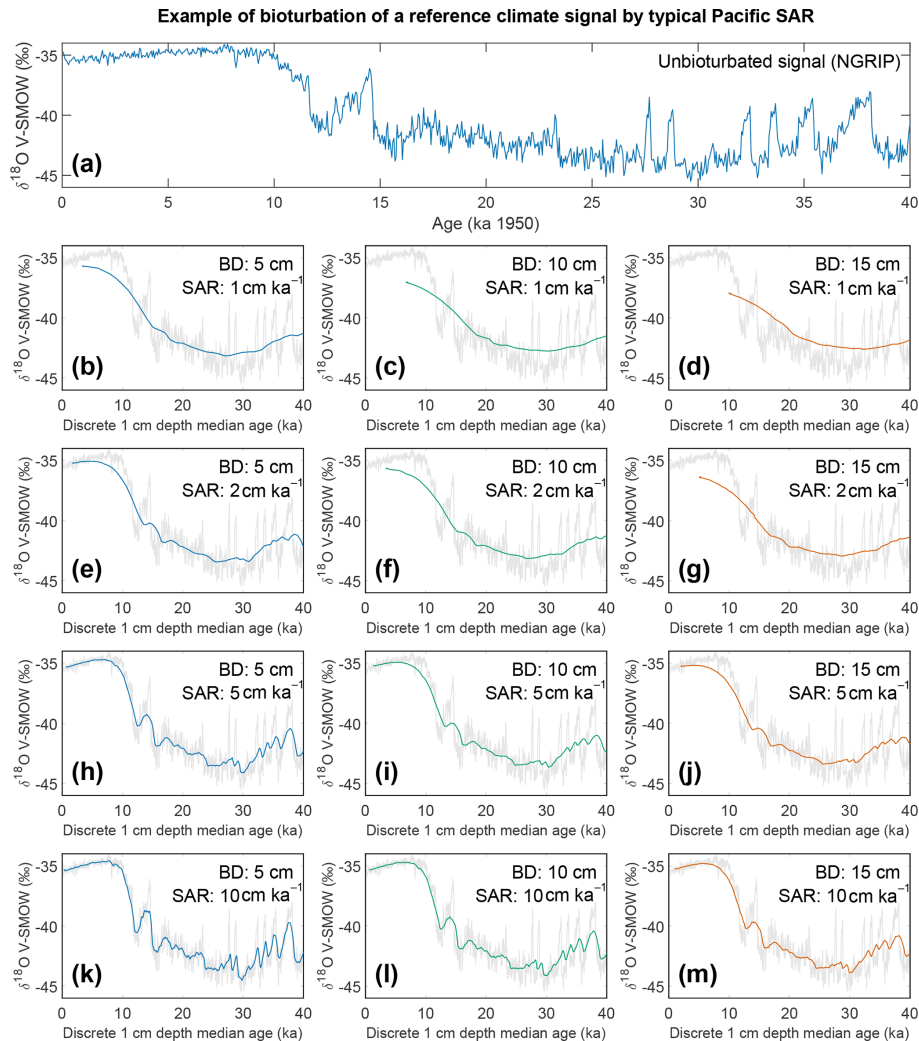


**Figure 8.** Output of the bioturbation model SEAMUS. **(a)** The unbioturbated input signal, NGRIP (North Greenland Ice Core Project Members, 2004; Rasmussen et al., 2014; Seierstad et al., 2014), used in our simulation of bioturbation for different SAR with SEAMUS (Lougheed, 2020b). Sediment mixed layer referred to here as bioturbation depth (BD) is fixed at **(b, e, h, k)** 5 cm, **(c, f, i, l)** 10 cm, and **(d, g, j, m)** 15 cm for sedimentation accumulation rates (SAR) of **(b–d)** 1 cm kyr<sup>-1</sup>, **(e–g)** 2 cm kyr<sup>-1</sup>, **(h–j)** 5 cm kyr<sup>-1</sup>, and **(k–m)** 10 cm kyr<sup>-1</sup>. The output is plotted as the discrete 1 cm depth median age. In **(b)–(m)** grey values represent the unbioturbated input signal, NGRIP. Note, we retain the original units (V-SMOW) of the original time series used; no inference between Pacific climate and Greenland is intended by the use of NGRIP.

spatially delineated El Niño events: the dateline central Pacific El Niño and the eastern Pacific El Niño. Here we have highlighted a way of using models to determine the location where the different climate states could be differentiated. More explicit tests using climate models could be used to optimise sampling design, determining applicable core locations for comparison of proxy values with “like with like” oceanographic features (similar to the analysis of Evans et al. (1998) for predicting coral sites), without necessarily the cost of a time-slice project (e.g. CLIMAP, MARGO).

Another test is whether for the same set of environmental conditions two species can record an identical signal. For species with a dynamic depth habitat in which the environ-

mental signal becomes a weighted average of the water column (e.g. Wilke et al., 2006) the likelihood of species recording the same environmental signal becomes less plausible. This is, in brief, the rationale for the development of FAME. The same climate signal seen through the view of species-specific proxies will give a fractured view constrained by each species ecophysiological constraints (Mix, 1987; Roche et al., 2018). FAME is not the first proxy system model; instead it expands upon previous studies that have either approximated a foraminiferal signal by weighting of ecological (seasonal or depth) preferences or assumed that foraminifera record a fixed depth in the water column. What can be seen as contradictory proxy reconstructions can therefore be viewed

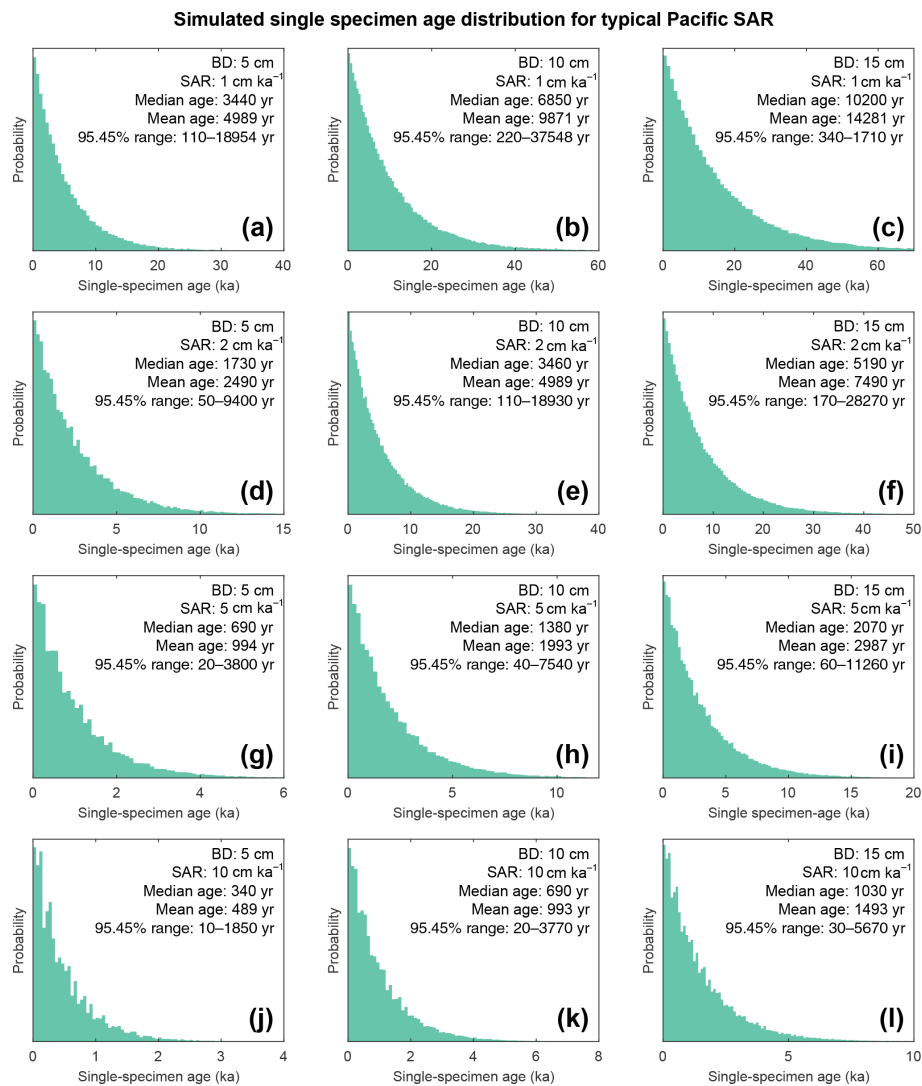


**Figure 9.** Histograms of simulated specimen age within the bioturbation depth. The simulated age distribution present within the sediment mixed layer, referred to here as bioturbation depth (BD). BD is fixed at (a, d, g, j) 5 cm, (b, e, h, k) 10 cm, and (c, f, i, l) 15 cm for sedimentation accumulation rates (SAR) of (a–c) 1 cm kyr<sup>-1</sup>, (d–f) 2 cm kyr<sup>-1</sup>, (g–i) 5 cm kyr<sup>-1</sup>, and (j–l) 10 cm kyr<sup>-1</sup>. The output is plotted as the discrete 1 cm depth median age. Note the size of the BD varies; therefore the simulated age distribution comes from a varying core depth.

as the prevailing or dominant conditions at a given location at the time when environmental conditions overlap with ecological constraints for a given species. Reconstructions of the past climate (LGM–Holocene) of the Pacific have for instance inferred a relatively weaker Walker circulation, a displaced intertropical convergence zone (ITCZ) and equatorial cooling (Koutavas and Lynch-Stieglitz, 2003), both a reduction (Koutavas and Lynch-Stieglitz, 2003) and intensification (Dubois et al., 2009) in eastern equatorial Pacific upwelling, and both weakened (Leduc et al., 2009) and strengthened ENSO variability (Koutavas and Joanides, 2012; Sadekov et al., 2013). However, a number of the inferences are contentious. For instance the reduction in upwelling in this re-

gion (Koutavas and Lynch-Stieglitz, 2003) is contradicted by Dubois et al. (2009), who used alkenones (i.e.  $U_{37}^{K'}$  ratios) to suggest an upwelling intensification. Whilst the  $U_{37}^{K'}$  proxy has problems within coastal upwelling sites (Kienast et al., 2012), it does not discount their claim, especially considering that  $\delta^{18}\text{O}$  records can themselves be influenced by salinity for the  $\delta^{18}\text{O}_{\text{sw}}$  component (Rincón-Martínez et al., 2011) and the potential influence of carbonate ion concentration,  $[\text{CO}_3^{2-}]$ , on foraminiferal  $\delta^{18}\text{O}_\text{c}$  (de Nooijer et al., 2009; Spero et al., 1997; Spero and Lea, 1996). The discrepancies in reconstructed climate between marine cores are worth noting, as ultimately it is from proxies that inferences are made about past climate (Trenberth and Otto-Bliesner,

2003; Rosenthal and Broccoli, 2004). Such inferences have suggested that the past climate of the Pacific region (from the geologically recent too deep time) has been in an El Niño state (Koutavas et al., 2002; Stott et al., 2002; Koutavas and Lynch-Stieglitz, 2003), a permanent El Niño state (Huber and Caballero, 2003), a super El Niño state (Stott et al., 2002), a La Niña state (Andreasen et al., 2001; Beaufort et al., 2001; Martinez et al., 2003), or a different climatic state altogether (Pisias and Mix, 1997; Feldberg and Mix, 2003). Ultimately the possibility of a marine sediment archive being able to reconstruct ENSO dynamics comes down to several fundamentals besides whether the signal can or cannot be preserved (i.e. whether the core site has too low a SAR, too high a BD, or a water depth not conducive to calcite preservation). These fundamentals are as follows: the time period captured by the sediment intervals (a combination of SAR and bioturbation), the frequency and intensity of ENSO events, the foraminiferal abundance during ENSO and non-ENSO conditions, and what the proxy is recording. Reconstructions of the past can benefit from inclusion within conceptual frameworks that incorporate both data and modelling studies (e.g. Trenberth and Otto-Bliesner, 2003; Rosenthal and Broccoli, 2004; McPhaden et al., 2006).

## 8.2 Limitations of the methods applied and assessment of model uncertainties

For simplicity we have assumed that our model is perfect; of course that is inaccurate, and there are four potential sources of error: the input variables (temperature, salinity, and their conversion into  $\delta^{18}\text{O}_{\text{sw}}$  and  $\delta^{18}\text{O}_{\text{eq}}$ ); the error of the model with respect to real-world values (Roche et al., 2018); the errors in the statistical test (associated Type I – in which attribution of significance is given to an insignificant random event, a false positive – and Type II – in which a significant event is attributed to be insignificant, a false negative – errors); and reducing the complexities of foraminiferal biology via parameterisation. The input variables can have errors associated with both the absolute values of temperature and salinity used here and the limitation of input values to a single value per month. Whilst it is possible to interpolate to a daily resolution, this is problematic for two reasons: (1) daily temperature records have much more high-frequency oscillations than the data here and (2) the life cycle of a single foraminifera is approximately monthly; therefore by using monthly data it provides an estimate of the average population signal. Conversion of salinity and temperature into  $\delta^{18}\text{O}_{\text{sw}}$  and  $\delta^{18}\text{O}_{\text{eq}}$  uses a quadratic approximation. One source of error is the unknown influence of carbonate ion concentration on both the Kim and O’Neil (1997) equation and the foraminiferal microenvironment (de Nooijer et al., 2008, 2009; Spero et al., 1997; Spero and DeNiro, 1987; Spero and Lea, 1996), which has implications due to the upwelling of cool, low-pH, waters in the eastern tropical Pacific (Cole and Tudhope, 2017; Raven et al., 2005). The spatial

variability in salinity, particularly within regions underlying the intertropical convergence zone (ITCZ) and the moisture transport from the Caribbean into the eastern Pacific along the topographic low that represents Panama Isthmus, and the resultant conversion of salinity to  $\delta^{18}\text{O}_{\text{sw}}$  and then  $\delta^{18}\text{O}_{\text{eq}}$  may contain further errors. If such errors are independent of the absolute value of the variable, i.e. the error on cold temperature is the same and not larger than warm temperatures, then the error terms effectively cancel one another out. A point of note is that the  $\delta^{18}\text{O}$  to  $^{\circ}\text{C}$  conversion of Kim and O’Neil (1997) is considered to be marginally larger at the cold end than at the warm end (0.2‰ per  $1^{\circ}\text{C}$  to 0.22‰ per  $1^{\circ}\text{C}$ ) than that which was originally discerned (O’Neil et al., 1969).

The comparison of the pseudo-Mg/Ca temperature signal produced here ( $T_c$ ) to a value corresponding to that reconstructed from measurements of Mg/Ca should be done with caution. Computation of pseudo-foraminiferal  $\delta^{18}\text{O}$  in FAME is aided by the ability to compute an initial  $\delta^{18}\text{O}$  equilibrium value for a given latitude–longitude grid point and time step. The weighting of  $\delta^{18}\text{O}$  value used in FAME is an approximation of the foraminiferal shell, chambers being generally homogenous in  $\delta^{18}\text{O}$  value, excluding either terminal features such as crust or gametogenic calcite which can lead to chamber heterogeneities (e.g. Wycech et al., 2018), although the latter can be approximated with an additional parameter (Roche et al., 2018). The same cannot be said for Mg/Ca. Alongside heterogeneities in the shell which may be the result of diurnal processes, there are differences in both sample preparation and measurement techniques. Whilst the change in Mg/Ca with temperature has been validated (e.g. Elderfield and Ganssen, 2000) the computation of a pseudo-proxy value for and from model parameters remains enigmatic. Construction of a matrix of equilibrium Mg/Ca would ideally be the most logical step in a second generation of the FAME model. Whilst simply solving the Mg/Ca palaeotemperature equation for an input of  $T$  and an output Mg/Ca is a first approximation, as stated previously several other parameters can alter this technique. This includes abiotic effects such as salinity (Allen et al., 2016; Gray et al., 2018; Groeneweld et al., 2008; Kısakürek et al., 2008) or carbonate ion concentration (Allen et al., 2016; Evans et al., 2018; Zeebe and Sanyal, 2002), biotic effects such as diurnal calcification (Eggins et al., 2003; Hori et al., 2018; Sadekov et al., 2008, 2009; Vetter et al., 2013), or additional factors such as sediment (Fallet et al., 2009; Feldmeijer et al., 2013) or specimen (Barker et al., 2003; Greaves et al., 2005) “cleaning” techniques. Given the role of Mg in inhibiting calcium carbonate formation, the manipulation of seawater, similar to the modification of the pH of a cell (de Nooijer et al., 2008, 2009), may aid calcification and explain the formation of low-Mg by certain foraminifera (Zeebe and Sanyal, 2002). Scaling these processes up to a basin-wide model is beyond the remit of this current paper.

Our modelling results also depend upon potential genotypes and the presence and type of symbionts of a species. For instance, mixotrophs, those organisms that utilise a mixture of sources for energy and carbon (planktonic foraminifera such as *G. ruber*; and/or *G. sacculifer*), can outcompete heterotrophic (or photoheterotrophic) organisms (planktonic foraminifera such as *Neogloboquadrina pachyderma* or *Neogloboquadrina incompta*), especially in stratified–oligotrophic waters. Whilst FAME uses only the temperature component of FORAMCLIM (Roche et al., 2018), it is important to note that there are distinctions between the fundamental niche that FAME computes, i.e. the conditions that an organism can survive, and the realised niche, i.e. what an organism actually occupies given limiting factors within the environment. As FORAMCLIM and therefore FAME are based upon culture experiments, new observations highlight symbiotic or species associations (see Bird et al., 2018, 2017). A species that hosts symbionts will likely have a restricted temperature that is associated with the temperature tolerance of their symbionts. Likewise, cryptic speciation may lead to foraminiferal genotypes exhibiting distinct environmental preferences (Bird et al., 2018, 2017; Darling et al., 2004, 2000, 1999; Huber et al., 1997; Morard et al., 2013; de Vargas et al., 1999, 2002). Incorporation of both a theoretical genotype abundance (Morard et al., 2013) and ecophysiological tolerances of different genotypes (Bird et al., 2018) within an ecophysiological model could further reduce error within modelling of planktonic foraminiferal habitats and thus reduce data–model comparison error. For instance, Morard et al. (2013) simulated the impact of genotypes upon palaeoceanographic reconstructions (in particular transfer functions) using a theoretical abundance, calculated with a best-fit Gaussian response model, depending upon SST, and later using a similar approach (Morard et al., 2016) to deduce the impact upon  $\delta^{18}\text{O}$ .

## 9 Conclusion

Concentrating on the period spanning the instrumental record, we forward modelled the species-specific (i.e. *G. ruber*; *G. sacculifer* and *N. dutertrei*) oxygen isotope values ( $\delta^{18}\text{O}_c$ ) and pseudo-temperature ( $T_c$ ), computed from ocean reanalysis data using the temperature driven FAME module. The aim of this study was to determine whether the modelled values from different climate states are statistically different. If our assumptions are correct, including the reduction in foraminiferal complexity and the choice of generic distribution (i.e. kernel) to the fit the data prior to performing an Anderson–Darling test, our results suggest that for large expanses of the tropical Pacific the climate states do have different values. Whilst the results show that the values between El Niño states and neutral climate states are statistically different for a large portion of the tropical Pacific, the total variance is dominated by the interannual variance for much of the

region. Overlaying our computed foraminiferal distributions with the characteristics of the Pacific Ocean we infer that much of the region available for reconstructions corresponds to areas where several processes will alter the preservation of the foraminiferal signal. First, the inferred SAR for much of the region is critically low, and a simulation of bioturbation for different bioturbation depths and SAR typical for the Pacific indicates that discrete core depths can have a large temporal spread in single foraminifera, possibly precluding the extraction of ENSO-related climate variability. Second, a large proportion of the seafloor lies below the lysocline, the depth at which dissolution of foraminifera becomes apparent. These factors reduce the size of the area available for reconstructions considerably, thus arguably precluding the extraction of a temporally valid palaeoclimate signal using long-standing methods. It is our inference that only at exceptional ocean sediment core sites is it possible to determine the variability in ENSO based on planktonic foraminifer measurements, which makes it difficult to build a Pacific basin-wide understanding of past ENSO dynamics.

**Code and data availability.** The ocean reanalysis data used in this paper are available from the Universität Hamburg. An open-source version of the FAME code is available from Roche et al. (2018). Statistical routines are available as part of the statistical package of MATLAB; mapping tools (including the topographic colour map) are part of the Mapping Toolbox. The function to retrieve GEBCO bathymetry (data available at <https://www.gebco.net/>, last access: 21 December 2017, GEBCO, 2015) from netcdf format, `gebconetcdf(FILE,Wlon,Elon,Slat,Nlat)`, is available from <https://github.com/bryanlougheed/gebconetcdf> (last access: 22 April 2020, Lougheed, 2020a). The single-foraminifera SEdiment AccuMulation Simulator (SEAMUS) is published in Lougheed (2020), available at <https://doi.org/10.5194/gmd-13-155-2020>. A video of the  $\delta^{18}\text{O}_{\text{shell}}$  output has been archived online (<https://doi.org/10.5281/zenodo.2554843>, Metcalfe et al., 2019b).

**Supplement.** The supplement related to this article is available online at: <https://doi.org/10.5194/cp-16-885-2020-supplement>.

**Author contributions.** BM and DMR designed the study. BM analysed the data. BCL processed ocean SAR and depth data and ran the bioturbation model. BM drafted the paper with contributions from all authors.

**Competing interests.** The authors declare that they have no conflict of interest.

**Acknowledgements.** Brett Metcalfe thanks both LSCE and VU Amsterdam for guest status. Bryan C. Lougheed acknowledges the Swedish National Infrastructure for Computing (SNIC) at the Uppsala Multidisciplinary Centre for Advanced Computational Science

(UPPMAX) that provided computer resources for running the SEAMUS model. We thank the Universität Hamburg for their online access server for ocean reanalysis data.

**Financial support.** This research has been supported by the European Commission, Seventh Framework Programme (ACCLIMATE; grant no. 339108). Brett Metcalfe was supported by a Laboratoire d'excellence (LabEx) of the Institut Pierre-Simon Laplace (Labex L-IPSL), funded by the French Agence Nationale de la Recherche (grant no. ANR-10-LABX-0018). Didier M. Roche is supported by the French agency Centre National de la Recherche Scientifique (CNRS) and VU Amsterdam. This is a contribution to the ACCLIMATE ERC project. The research leading to these results has received funding to Claire Waelbroeck from the European Research Council under the European Commission, Seventh Framework Programme (grant no. 339108). Bryan C. Lougheed acknowledges Swedish Research Council (Vetenskapsrådet – VR) (grant no. 2018-04992).

**Review statement.** This paper was edited by Eric Wolff and reviewed by Michal Kucera and four anonymous referees.

## References

- Allen, K. A., Hönisch, B., Eggins, S. M., Haynes, L. L., Rosenthal, Y., and Yu, J.: Trace element proxies for surface ocean conditions: A synthesis of culture calibrations with planktic foraminifera, *Geochim. Cosmochim. Ac.*, 193, 197–221, <https://doi.org/10.1016/j.gca.2016.08.015>, 2016.
- An, S.-I. and Bong, H.: Inter-decadal change in El Niño-Southern Oscillation examined with Bjerknes stability index analysis, *Clim. Dynam.*, 47, 967–979, <https://doi.org/10.1007/s00382-015-2883-8>, 2016.
- An, S.-I. and Bong, H.: Feedback process responsible for the suppression of ENSO activity during the mid-Holocene, *Theor. Appl. Climatol.*, 132, 779–790, <https://doi.org/10.1007/s00704-017-2117-6>, 2018.
- Anderson, T. W. and Darling, D. A.: A test of goodness of fit, *J. Am. Stat. Assoc.*, 49, 765–769, <https://doi.org/10.2307/2281537>, 1954.
- Andreasen, D. H., Ravelo, A. C., and Broccoli, A. J.: Remote forcing at the Last Glacial Maximum in the tropical Pacific Ocean, *J. Geophys. Res.*, 106, 879–897, 2001.
- Balmaseda, M. A., Mogensen, K., and Weaver, A. T.: Evaluation of the ECMWF ocean reanalysis system ORAS4, *Q. J. Roy. Meteor. Soc.*, 139, 1132–1161, 2013.
- Barker, S., Greaves, M., and Elderfield, H.: A study of cleaning procedures used for foraminiferal Mg/Ca paleothermometry, *Geochem. Geophys. Geosy.*, 4, 8407, <https://doi.org/10.1029/2003GC000559>, 2003.
- Batiza, R.: Abundances, distribution and sizes of volcanoes in the Pacific Ocean and implications for the origin of non-hotspot volcanoes, *Earth Planet. Sc. Lett.*, 60, 195–206, 1982.
- Bé, A. W. H. and Spero, H. J.: Shell regeneration and biological recovery of planktonic foraminifera after physical injury induced in laboratory culture, *Micropaleontology*, 27, 305–316, 1981.
- Bé, A. W. H., Spero, H. J., and Anderson, O. R.: Effects of symbiont elimination and reinfection on the life processes of the planktonic foraminifer *Globigerinoides sacculifer*, *Mar. Biol.*, 70, 73–86, 1982.
- Beaufort, L., Garidel-Thoron, T., Mix, A. C., and Pisias, N. G.: ENSO like forcing on oceanic primary production during the late Pleistocene, *Science*, 293, 2440–2444, 2001.
- Bemis, B. E., Spero, H. J., Bijma, J., and Lea, D. W.: Reevaluation of the oxygen isotopic composition of planktonic foraminifera: Experimental results and revised paleotemperature equations, *Paleoceanography*, 13, 150–160, <https://doi.org/10.1029/98PA00070>, 1998.
- Berger, W. H.: Planktonic Foraminifera: selective solution and paleoclimatic interpretation, *Deep-Sea Res.*, 15, 31–43, 1968.
- Berger, W. H.: Sedimentation of planktonic foraminifera, *Mar. Geol.*, 11, 325–358, [https://doi.org/10.1016/0025-3227\(71\)90035-1](https://doi.org/10.1016/0025-3227(71)90035-1), 1971.
- Berger, W. H. and Heath, G. R.: Vertical mixing in pelagic sediments, *J. Mar. Res.*, 26, 134–143, 1968.
- Berger, W. H., Adelseck, C., and Mayer, L. A.: Distribution of carbonate in surface sediments of the Pacific, *J. Geophys. Res.*, 81, 2617–2627, <https://doi.org/10.1029/JC081i015p02617>, 1976.
- Bijma, J., Hönisch, B., and Zeebe, R. E.: Impact of the ocean carbonate chemistry on living foraminiferal shell weight: Comment on “Carbonate ion concentration in glacial-age deep waters of the Caribbean Sea” by W. S. Broecker and E. Clark, *Geochem. Geophys.*, 3, 1–7, <https://doi.org/10.1029/2002GC000388>, 2002.
- Bird, C., Darling, K. F., Russell, A. D., Davis, C. V., Fehrenbacher, J., Free, A., Wyman, M., and Ngwenya, B. T.: Cyanobacterial endobionts within a major marine planktonic calcifier (*Globigerina bulloides*, Foraminifera) revealed by 16S rRNA metabarcoding, *Biogeosciences*, 14, 901–920, <https://doi.org/10.5194/bg-14-901-2017>, 2017.
- Bird, C., Darling, K. F., Russell, A. D., Fehrenbacher, J. S., Davis, C. V., Free, A., and Ngwenya, B. T.: 16S rRNA gene metabarcoding and TEM reveals different ecological strategies within the genus *Neogloboquadrina* (planktonic foraminifer), *PLOS ONE*, 13, e0191653, <https://doi.org/10.1371/journal.pone.0191653>, 2018.
- Blackman, A. and Somayajulu, B. L. K.: Pacific Pleistocene Cores: Faunal Analyses and Geochronology, *Science*, 154, 886–889, 1966.
- Boudreau, B. P.: Mean mixed depth of sediments: The wherefore and the why, *Limnol. Oceanogr.*, 43, 524–526, 1998.
- Bramlette, M. N.: Pelagic sediments, in: *Oceanography*, edited by: Sears, M., American Association Advancement of Science, Washington, D.C., Publication 67, <https://doi.org/10.5962/bhl.title.34806>, 1961.
- Brand, W. A., Coplen, T. B., Vogl, J., Rosner, M., and Prohaska, T.: Assessment of international reference materials for isotope-ratio analysis (IUPAC Technical Report), *Pure Appl. Chem.*, 86, 425–467, <https://doi.org/10.1515/pac-2013-1023>, 2014.
- Caley, T., Roche, D. M., Waelbroeck, C., and Michel, E.: Oxygen stable isotopes during the Last Glacial Maximum climate: perspectives from data–model (iLOVECLIM) comparison, *Clim. Past*, 10, 1939–1955, <https://doi.org/10.5194/cp-10-1939-2014>, 2014.

- Carton, J. A., Chepurin, G. A., Cao, X., and Giese, B. S.: A Simple Ocean Data Assimilation analysis of the global upper ocean 1950–1995, Part 1: methodology, *J. Phys. Oceanogr.*, 30, 294–309, 2000a.
- Carton, J. A., Chepurin, G. A., and Cao, X.: A Simple Ocean Data Assimilation analysis of the global upper ocean 1950–1995 Part 2: results, *J. Phys. Oceanogr.*, 30, 311–326, 2000b.
- Clement, A. C., Seager, R., and Cane, M. A.: Orbital controls on the El Niño/Southern Oscillation and the tropical climate, *Paleoceanography*, 14, 441–456, 1999.
- Clouard, V. and Bonneville, A.: Ages of seamounts, islands, and plateaus on the Pacific plate, *Geol. S. Am. S.*, 388, 71–90, <https://doi.org/10.1130/0-8137-2388-4.71>, 2005.
- Cole, J. E. and Tudhope, A. W.: Reef-based reconstructions of eastern Pacific climate variability, in: *Coral Reefs of the Eastern Pacific: Persistence and Loss in a Dynamic Environment*, edited by: Glynn, P. W. and Manzello, D., Springer, The Netherlands, 535–549, [https://doi.org/10.1007/978-94-017-7499-4\\_19](https://doi.org/10.1007/978-94-017-7499-4_19), 2017.
- Coplen, T. B.: Reporting of stable carbon, hydrogen, and oxygen isotopic abundances, Reference and intercomparison materials for stable isotopes of light elements, IAEA, Vienna, Austria, 1–3 December 1993, 159 pp., 1995.
- Darling, K. F., Wade, C. M., Kroon, D., Brown, A. J. L., and Bijma, J.: The Diversity and Distribution of Modern Planktic Foraminiferal Small Subunit Ribosomal RNA Genotypes and their Potential as Tracers of Present and Past Ocean Circulations, *Paleoceanography*, 14, 3–12, <https://doi.org/10.1029/1998PA900002>, 1999.
- Darling, K. F., Wade, C. M., Steward, I. A., Kroon, D., Dingle, R., and Leigh Brown, A. J.: Molecular evidence for genetic mixing of Arctic and Antarctic subpolar populations of planktonic foraminifera, *Nature*, 405, 43–47, 2000.
- Darling, K. F., Kucera, M., Pudsey, C. J., and Wade, C. M.: Molecular evidence links cryptic diversification in polar planktonic protists to Quaternary climate dynamics, *P. Natl. Acad. Sci.*, 101, 7657–7662, <https://doi.org/10.1073/pnas.0402401101>, 2004.
- Dee, S., Emile-Geay, J., Evans, M. N., Allam, A., Steig, E. J., and Thompson, D. M.: PRYSM: An open-source framework for PROXY System Modeling, with applications to oxygen-isotope systems, *J. Adv. Model. Earth Sy.*, 7, 1220–1247, <https://doi.org/10.1002/2015MS000447>, 2015.
- de Garidel-Thoron, T., Rosenthal, Y., Beaufort, L., Bard, E., Sonzogni, C., and Mix, A. C.: A multiproxy assessment of the western equatorial Pacific hydrography during the last 30 kyr, *Paleoceanography*, 22, <https://doi.org/10.1029/2006PA001269>, 2007.
- de Nooijer, L. J., Toyofuku, T., Oguri, K., Nomaki, H., and Kitazato, H.: Intracellular pH distribution in foraminifera determined by the fluorescent probe HPTS: Intracellular pH of foraminifera, *Limnol. Oceanogr.-Meth.*, 6, 610–618, <https://doi.org/10.4319/lom.2008.6.610>, 2008.
- de Nooijer, L. J., Toyofuku, T., and Kitazato, H.: Foraminifera promote calcification by elevating their intracellular pH, *P. Natl. Acad. Sci. USA*, 106, 15374–15378, <https://doi.org/10.1073/pnas.0904306106>, 2009.
- Deuser, W. G., Ross, E. H., and Anderson, R. F.: Seasonality in the supply of sediment to the deep Sargasso Sea and implications for the rapid transfer of matter to the deep ocean, *Deep-Sea Res.*, 28, 495–505, [https://doi.org/10.1016/0198-0149\(81\)90140-0](https://doi.org/10.1016/0198-0149(81)90140-0), 1981.
- de Vargas, C., Norris, R., Zaninetti, L., Gibb, S. W., and Pawlowski, J.: Molecular evidence of cryptic speciation in planktonic foraminifera and their relation to oceanic provinces, *P. Natl. Acad. Sci.*, 96, 2864–2868, <https://doi.org/10.1073/pnas.96.6.2864>, 1999.
- de Vargas, C., Bonzon, M., Rees, N. W., Pawlowski, J., and Zaninetti, L.: A molecular approach to biodiversity and biogeography in the planktonic foraminifer *Globigerinella siphonifera* (d’Orbigny), *Mar. Micropaleontol.*, 45, 101–116, 2002.
- Dolman, A. M. and Laepple, T.: Sedproxy: a forward model for sediment-archived climate proxies, *Clim. Past*, 14, 1851–1868, <https://doi.org/10.5194/cp-14-1851-2018>, 2018.
- Dubois, N., Kienast, M., Normandeau, C., and Herbert, T. D.: Eastern equatorial Pacific cold tongue during the Last Glacial Maximum as seen from alkenone paleothermometry, *Paleoceanography*, 24, PA4207, <https://doi.org/10.1029/2009PA001781>, 2009.
- Eggins, S. M., Sadekov, A., and de Deckker, P.: Modulation and daily banding of Mg/Ca in *Orbulina universa* tests by symbiont photosynthesis and respiration: a complication for seawater thermometry, *Earth Planet. Sc. Lett.*, 225, 411–419, 2003.
- Elderfield, H. and Ganssen, G. M.: Past temperature and  $\delta^{18}\text{O}$  of surface ocean waters inferred from foraminiferal Mg/Ca ratios, *Nature*, 405, 442–445, 2000.
- Evans, M. N., Kaplan, A., and Cane, M. A.: Optimal sites for coral-based reconstructions of global sea surface temperature, *Paleoceanography*, 13, 502–516, 1998.
- Evans, M. N., Tolwinski-Ward, S. E., Thompson, D. M., and Anchukaitis, K. J.: Applications of proxy system modeling in high resolution paleoclimatology, *Quaternary Sci. Rev.*, 76, 16–28, <https://doi.org/10.1016/j.quascirev.2013.05.024>, 2013.
- Evans, D., Müller, W., and Erez, J.: Assessing foraminifera biomineralisation models through trace element data of cultures under variable seawater chemistry, *Geochim. Cosmochim. Ac.*, 236, 198–217, <https://doi.org/10.1016/j.gca.2018.02.048>, 2018.
- Fallet, U., Boer, W., van Assen, C., Greaves, M., and Brummer, G. J. A.: A novel application of wet-oxidation to retrieve carbonates from large, organic-rich samples for application in climate research, *Geochem. Geophys. Geosy.*, 10, Q08004, <https://doi.org/10.1029/2009GC002573>, 2009.
- Feldberg, M. J. and Mix, A. C.: Planktonic foraminifera, sea surface temperatures, and mechanisms of oceanic change in the Peru and south equatorial currents, 0–150 ka BP, *Paleoceanography*, 18, 1–16, 2003.
- Feldmeijer, W., Metcalfe, B., Scussolini, P., and Arthur, K.: The effect of chemical pretreatment of sediment upon foraminiferal-based proxies, *Geochem. Geophys. Geosy.*, 14, 3996–4014, <https://doi.org/10.1002/ggge.20233>, 2013.
- Feldmeijer, W., Metcalfe, B., Brummer, G. J. A., and Ganssen, G. M.: Reconstructing the depth of the permanent thermocline through the morphology and geochemistry of the deep dwelling planktonic foraminifer *Globorotalia truncatulinoides*, *Paleoceanography*, 30, 1–22, <https://doi.org/10.1002/2014PA002687>, 2015.
- Ford, H. L., Ravelo, A. C., and Polissar, P. J.: Reduced El Niño–Southern Oscillation during the Last Glacial Maximum, *Science*, 347, 255–258, <https://doi.org/10.1126/science.1258437>, 2015.
- Fraass, A. J. and Lowery, C. M.: Defining uncertainty and error in planktic foraminiferal oxygen iso-

- tope measurements, *Paleoceanography*, 32, 104–122, <https://doi.org/10.1002/2016PA003035>, 2017.
- Fraile, I., Schulz, M., Mulitza, S., and Kucera, M.: Predicting the global distribution of planktonic foraminifera using a dynamic ecosystem model, *Biogeosciences*, 5, 891–911, <https://doi.org/10.5194/bg-5-891-2008>, 2008.
- Fraile, I., Schulz, M., Mulitza, S., Merkel, U., Prange, M., and Paul, A.: Modeling the seasonal distribution of planktonic foraminifera during the Last Glacial Maximum, *Paleoceanography*, 24, PA2216, <https://doi.org/10.1029/2008PA001686>, 2009.
- GEBCO (General Bathymetric Chart of the Oceans): GEBCO\_2014 Grid, version 20150318, available at: <https://www.gebco.net/> (last access: 21 December 2017), 2015.
- Gray, W. R., Weldeab, S., Lea, D. W., Rosenthal, Y., Gruber, N., Donner, B., and Fischer, G.: The effects of temperature, salinity, and the carbonate system on Mg/Ca in *Globigerinoides ruber* (white): A global sediment trap calibration, *Earth Planet. Sc. Lett.*, 482, 607–620, <https://doi.org/10.1016/j.epsl.2017.11.026>, 2018.
- Greaves, M., Barker, S., Daunt, C., and Elderfield, H.: Accuracy, standardization, and interlaboratory calibration standards for foraminiferal Mg/Ca thermometry, *Geochem. Geophys. Geosyst.*, 6, Q02D13, <https://doi.org/10.1029/2004GC000790>, 2005.
- Groeneveld, J., Nürnberg, D., Tiedemann, R., Reichert, G.-J., Steph, S., Reuning, L., Crudeli, D., and Mason, P.: Foraminiferal Mg/Ca increase in the Caribbean during the Pliocene: Western Atlantic Warm Pool formation, salinity influence, or diagenetic overprint?, *Geochem. Geophys. Geosyst.*, 9, Q01P23, <https://doi.org/10.1029/2006GC001564>, 2008.
- Hamilton, C. P., Spero, H. J., Bijma, J., and Lea, D. W.: Geochemical investigation of gametogenic calcite addition in the planktonic foraminifera *Orbulina universa*, *Mar. Micropaleontol.*, 68, 256–267, 2008.
- Hays, J. D., Saito, T., Opydyke, N., and Burckle, L. H.: Pliocene-Pleistocene Sediments of the Equatorial Pacific: Their Paleomagnetic, Biostratigraphic, and Climatic Record, *Geol. Soc. Am. Bull.*, 80, 1481–1514, 1969.
- Hillier, J. K.: Pacific seamount volcanism in space and time, *Geophys. J. Int.*, 168, 877–889, <https://doi.org/10.1111/j.1365-246X.2006.03250.x>, 2007.
- Hori, M., Shirai, K., Kimoto, K., Kurasawa, A., Takagi, H., Ishida, A., Takahata, N., and Sano, Y.: Chamber formation and trace element distribution in the calcite walls of laboratory cultured planktonic foraminifera (*Globigerina bulloides* and *Globigerinoides ruber*), *Mar. Micropaleontol.*, 140, 46–55, <https://doi.org/10.1016/j.marmicro.2017.12.004>, 2018.
- Huang, B., Thorne, P. W., Banzon, V. F., Boyer, T., Chepurin, G., Lawrimore, J. H., Menne, M. J., Smith, T. M., Vose, R. S., and Zhang, H.-M.: Extended Reconstructed Sea Surface Temperature, Version 5 (ERSSTv5): Upgrades, Validations, and Intercomparisons, *J. Climate*, 30, 8179–8205, <https://doi.org/10.1175/jcli-d-16-0836.1>, 2017.
- Huber, B. T., Bijma, J., and Darling, K.: Cryptic speciation in the living planktonic foraminifer *Globigerinella siphonifera* (d’Orbigny), *Paleobiology*, 23, 33–62, <https://doi.org/10.1017/S0094837300016638>, 1997.
- Huber, M. and Caballero, R.: Eocene El Niño: Evidence for Robust Tropical Dynamics in the “Hothouse”, *Science*, 299, 877–881, 2003.
- Hut, G.: Consultants group meeting on stable isotope reference samples for geochemical and hydrological investigations, International Atomic Energy Agency, Vienna, 1987.
- Jonkers, L. and Kučera, M.: Quantifying the effect of seasonal and vertical habitat tracking on planktonic foraminifera proxies, *Clim. Past*, 13, 573–586, <https://doi.org/10.5194/cp-13-573-2017>, 2017.
- Kageyama, M., Braconnot, P., Bopp, L., Caubel, A., Foujols, M.-A., Guilyardi, E., Khodri, M., Lloyd, J., Lombard, F., Mariotti, V., Marti, O., Roy, T., and Woille, M.-N.: Mid-Holocene and Last Glacial Maximum climate simulations with the IPSL model—part I: comparing IPSL\_CM5A to IPSL\_CM4, *Clim. Dynam.*, 40, 2447–2468, <https://doi.org/10.1007/s00382-012-1488-8>, 2013.
- Keigwin, L. D. and Guilderson, T. P.: Bioturbation artifacts in zero-age sediments, *Paleoceanography*, 24, PA4212, <https://doi.org/10.1029/2008PA001727>, 2009.
- Kienast, M., MacIntyre, G., Dubois, N., Higginson, S., Normandeau, C., Chazen, C., and Herbert, T. D.: Alkenone unsaturation in surface sediments from the eastern equatorial Pacific: Implications for SST reconstructions, *Paleoceanography*, 27, PA1210, <https://doi.org/10.1029/2011PA002254>, 2012.
- Kim, S.-T. and O’Neil, J. R.: Equilibrium and nonequilibrium oxygen isotope effects in synthetic carbonates, *Geochim. Cosmochim. Ac.*, 61, 3461–3475, [https://doi.org/10.1016/S0016-7037\(97\)00169-5](https://doi.org/10.1016/S0016-7037(97)00169-5), 1997.
- Kisakürek, B., Eisenhauer, A., Böhm, F., Garbe-Schönberg, D., and Erez, J.: Controls on shell Mg/Ca and Sr/Ca in cultured planktonic foraminifera, *Globigerinoides ruber* (white), *Earth Planet. Sc. Lett.*, 273, 260–269, <https://doi.org/10.1016/j.epsl.2008.06.026>, 2008.
- Koppers, A. A. P., Staudigel, H., Pringle, M. S., and Wijbrans, J. R.: Short-lived and discontinuous intraplate volcanism in the South Pacific; hot spots or extensional volcanism, *Geochem. Geophys. Geosyst.*, 4, 1089, <https://doi.org/10.1029/2003GC000533>, 2003.
- Koutavas, A. and Joanides, S.: El Niño–Southern Oscillation extrema in the Holocene and Last Glacial Maximum, *Paleoceanography*, 27, PA4208, <https://doi.org/10.1029/2012PA002378>, 2012.
- Koutavas, A. and Lynch-Stieglitz, J.: Glacial-interglacial dynamics of the eastern equatorial Pacific cold tongue–Intertropical Convergence Zone system reconstructed from oxygen isotope records, *Paleoceanography*, 18, 1089, <https://doi.org/10.1029/2003PA000894>, 2003.
- Koutavas, A., Lynch-Stieglitz, J., Marchitto, T. M., and Sachs, J. P.: El Niño-Like Pattern in Ice Age Tropical Pacific Sea Surface Temperature, *Science*, 297, 226–230, <https://doi.org/10.1126/science.1072376>, 2002.
- Koutavas, A., deMenocal, P. B., Olive, G. C., and Lynch-Stieglitz, J.: Mid-Holocene El Niño–Southern Oscillation (ENSO) attenuation revealed by individual foraminifera in eastern tropical Pacific sediments, *Geology*, 34, 993–996, <https://doi.org/10.1130/G22810A.1>, 2006.
- Kretschmer, K., Kucera, M., and Schulz, M.: Modeling the distribution and seasonality of *Neogloboquadrina pachyderma* in the North Atlantic Ocean during Heinrich Stadial 1, *Paleoceanog-*



- raphy, 31, 986–1010, <https://doi.org/10.1002/2015PA002819>, 2016.
- Kretschmer, K., Jonkers, L., Kucera, M., and Schulz, M.: Modeling seasonal and vertical habitats of planktonic foraminifera on a global scale, *Biogeosciences*, 15, 4405–4429, <https://doi.org/10.5194/bg-15-4405-2018>, 2018.
- Leduc, G., Vidal, L., Cartapanis, O., and Bard, E.: Modes of eastern equatorial Pacific thermocline variability: Implications for ENSO dynamics over the last glacial period, *Paleoceanography*, 24, PA3202, <https://doi.org/10.1029/2008PA001701>, 2009.
- LeGrande, A. N. and Schmidt, G. A.: Global gridded data set of the oxygen isotopic composition in seawater, *Geophys. Res. Lett.*, 33, L12604, <https://doi.org/10.1029/2006GL026011>, 2006.
- Lombard, F., Labeyrie, L., Michel, E., Spero, H. J., and Lea, D. W.: Modelling the temperature dependent growth rates of planktic foraminifera, *Mar. Micropalaeontol.*, 70, 1–7, 2009.
- Lombard, F., da Rocha, R. E., Bijma, J., and Gattuso, J.-P.: Effect of carbonate ion concentration and irradiance on calcification in planktonic foraminifera, *Biogeosciences*, 7, 247–255, <https://doi.org/10.5194/bg-7-247-2010>, 2010.
- Lombard, F., Labeyrie, L., Michel, E., Bopp, L., Cortijo, E., Retailliau, S., Howa, H., and Jorissen, F.: Modelling planktic foraminifer growth and distribution using an ecophysiological multi-species approach, *Biogeosciences*, 8, 853–873, <https://doi.org/10.5194/bg-8-853-2011>, 2011.
- Lougheed, B. C.: *gebconetcdf.m*, available at: <https://github.com/bryanlougheed/gebconetcdf>, last access: 22 April 2020a.
- Lougheed, B. C.: SEAMUS (v1.20): a  $\Delta^{14}\text{C}$ -enabled, single-specimen sediment accumulation simulator, *Geosci. Model Dev.*, 13, 155–168, <https://doi.org/10.5194/gmd-13-155-2020>, 2020b.
- Lougheed, B. C., Metcalfe, B., Ninnemann, U. S., and Wacker, L.: Moving beyond the age–depth model paradigm in deep-sea palaeoclimate archives: dual radiocarbon and stable isotope analysis on single foraminifera, *Clim. Past*, 14, 515–526, <https://doi.org/10.5194/cp-14-515-2018>, 2018.
- Lougheed, B. C., Ascough, P., Dolman, A. M., Löwemark, L., and Metcalfe, B.: Re-evaluating  $^{14}\text{C}$  dating accuracy in deep-sea sediment archives, *Geochronology*, 2, 17–31, <https://doi.org/10.5194/gchron-2-17-2020>, 2020.
- Martínez, I., Keigwin, L., Barrows, T. T., Yokoyama, Y., and Southon, J.: La Niña-like conditions in the eastern equatorial Pacific and a stronger Choco jet in the northern Andes during the last glaciation, *Paleoceanography*, 18, 1033, <https://doi.org/10.1029/2002PA000877>, 2003.
- McPhaden, M. J., Zebiak, S. E., and Glantz, M. H.: ENSO as an Integrating Concept in Earth Science, *Science*, 314, 1740–1745, 2006.
- Menard, H. W.: *Marine Geology of the Pacific*, McGraw-Hill, New York, 1964.
- Metcalfe, B., Feldmeijer, W., de Vringer-Picon, M., Brummer, G.-J. A., Peeters, F. J. C., and Ganssen, G. M.: Late Pleistocene glacial–interglacial shell-size–isotope variability in planktonic foraminifera as a function of local hydrography, *Biogeosciences*, 12, 4781–4807, <https://doi.org/10.5194/bg-12-4781-2015>, 2015.
- Metcalfe, B., Feldmeijer, W., and Ganssen, G. M.: Oxygen isotope variability of planktonic foraminifera provide clues to past upper ocean seasonal variability, *Paleoceanography and Paleoclimatology*, 34, 374–393, <https://doi.org/10.1029/2018PA003475>, 2019a.
- Metcalfe, B., Lougheed, B. C., Waelbroeck, C., and Roche, D. M.: On the validity of foraminifera-based ENSO reconstructions, Version 1.0.0, Zenodo, <https://doi.org/10.5281/zenodo.2554843>, 2019b.
- Mikis, A., Hendry, K. R., Pike, J., Schmidt, D. N., Edgar, K. M., Peck, V., Peeters, F. J. C., Leng, M. J., Meredith, M. P., Todd, C. L., Stammerjohn, S., and Ducklow, H.: Temporal variability in foraminiferal morphology and geochemistry at the West Antarctic Peninsula: a sediment trap study, *Biogeosciences*, 16, 3267–3282, <https://doi.org/10.5194/bg-16-3267-2019>, 2019.
- Mix, A. C.: The oxygen-isotope record of deglaciation, in: *North America and adjacent oceans during the last deglaciation*, in *The Geology of America*, vol. K-3, edited by: Ruddiman, W. F. and Wright, H. E. J., Geological Society of America, Boulder, Colorado, 111–135, 1987.
- Morard, R., Quillévéré, F., Escarguel, G., de Garidel-Thoron, T., de Vargas, C., and Kucera, M.: Ecological modeling of the temperature dependence of cryptic species of planktonic Foraminifera in the Southern Hemisphere, *Palaeogeogr. Palaeoclimatol.*, 391, 13–33, <https://doi.org/10.1016/j.palaeo.2013.05.011>, 2013.
- Morard, R., Reinelt, M., Chiessi, C. M., Groeneveld, J., and Kucera, M.: Tracing shifts of oceanic fronts using the cryptic diversity of the planktonic foraminifera *Globorotalia inflata*, *Paleoceanography*, 31, 1193–1205, <https://doi.org/10.1002/2016PA002977>, 2016.
- Mulitza, S., Wolff, T., Pätzold, J., Hale, W., and Wefer, G.: Temperature sensitivity of planktic foraminifera and its influence on the oxygen isotope record, *Mar. Micropaleontol.*, 33, 223–240, [https://doi.org/10.1016/S0377-8398\(97\)00040-6](https://doi.org/10.1016/S0377-8398(97)00040-6), 1998.
- Murray, J. and Renard, A. F.: Deep-sea deposits (based on the specimens collected during the voyage of HMS Challenger in the years 1872 to 1876), Report on the scientific results of the voyage of H.M.S. Challenger during the years 1873–76, John Menzies and Co., Edinburgh, United Kingdom, 1891.
- North Greenland Ice Core Project Members: High-resolution record of Northern Hemisphere climate extending into the Last Interglacial period, *Nature*, 431, 147–151, 2004.
- Nürnberg, D., Bijma, J., and Hemleben, C.: Assessing the reliability of magnesium in foraminiferal calcite as a proxy for water mass temperatures, *Geochim. Cosmochim. Ac.*, 60, 803–814, 1996.
- Olson, P., Reynolds, E., Hinnov, L., and Goswami, A.: Variation of ocean sediment thickness with crustal age, *Geochem. Geophys. Geosy.*, 17, 1349–1369, 2016.
- O’Neil, J. R., Clayton, R. N., and Mayeda, T. K.: Oxygen Isotope Fractionation in Divalent Metal Carbonates, *J. Chem. Phys.*, 51, 5547–5558, 1969.
- Parker, F. L. and Berger, W. H.: Faunal and solution patterns of planktonic Foraminifera in surface sediments of the South Pacific, *Deep-Sea Res.*, 18, 73–107, 1971.
- Pena, L. D., Cacho, I., Ferretti, P., and Hall, M. A.: El Niño–Southern Oscillation-like variability during glacial terminations and interlatitudinal teleconnections, *Paleoceanography*, 23, PA3101, <https://doi.org/10.1029/2008PA001620>, 2008.
- Peng, T.-H., Broecker, W. S., and Berger, W. H.: Rates of benthic mixing in deep-sea sediment as determined by radioactive tracers, *Quaternary Res.*, 11, 141–149, 1979.
- Pisias, N. G. and Mix, A. C.: Aliasing of the geologic record and the search for long-period Milankovitch cycles, *Paleoceanography*, 3, 613–619, <https://doi.org/10.1029/PA003i005p00613>, 1988.

- Pisias, N. G. and Mix, A. C.: Spatial and temporal oceanographic variability of the eastern equatorial Pacific during the late Pleistocene: evidence from Radiolaria microfossils, *Paleoceanography*, 12, 381–393, 1997.
- Pracht, H., Metcalfe, B., and Peeters, F. J. C.: Oxygen isotope composition of the final chamber of planktic foraminifera provides evidence of vertical migration and depth-integrated growth, *Biogeosciences*, 16, 643–661, <https://doi.org/10.5194/bg-16-643-2019>, 2019.
- Rasmussen, S. O., Bigler, M., Blockley, S., Blunier, T., Buchardt, B., Clausen, H., Cvijanovic, I., Dahl-Jensen, D., Johnsen, S., Fischer, H., Gkinis, V., Guillevic, M., Hoek, W., Lowe, J., Pedro, J., Popp, T., Seierstad, I., Steffensen, J., Svensson, A., Vallelonga, P., Vinther, B., Walker, M., Wheatley, J. J., and Winstrup, M.: A stratigraphic framework for abrupt climatic changes during the Last Glacial period based on three synchronized Greenland ice-core records: refining and extending the INTIMATE event stratigraphy, *Quaternary Sci. Rev.*, 106, 14–27, 2014.
- Raven, J., Caldeira, K., Elderfield, H., Hoegh-Guldberg, O., Liss, P. S., Riebesell, U., Sheperd, J., Turley, C., and Watson, A.: Ocean Acidification due to Increasing Atmospheric Carbon Dioxide, Royal Society, London, Royal Society Policy Document 12/05, 68 pp., 2005.
- Rincón-Martínez, D., Steph, S., Lamy, F., Mix, A., and Tiedemann, R.: Tracking the equatorial front in the eastern equatorial Pacific Ocean by the isotopic and faunal composition of planktonic foraminifera, *Mar. Micropaleontol.*, 79, 24–40, <https://doi.org/10.1016/j.marmicro.2011.01.001>, 2011.
- Rink, S., Kühl, M., Bijma, J., and Spero, H. J.: Microsensor studies of photosynthesis and respiration in the symbiotic foraminifer *Orbulina universa*, *Mar. Biol.*, 131, 583–595, 1998.
- Roche, D. M., Paillard, D., Caley, T., and Waelbroeck, C.: LGM hosing approach to Heinrich Event 1: results and perspectives from data–model integration using water isotopes, *Quaternary Sci. Rev.*, 106, 247–261, <https://doi.org/10.1016/j.quascirev.2014.07.020>, 2014.
- Roche, D. M., Waelbroeck, C., Metcalfe, B., and Caley, T.: FAME (v1.0): a simple module to simulate the effect of planktonic foraminifer species-specific habitat on their oxygen isotopic content, *Geosci. Model Dev.*, 11, 3587–3603, <https://doi.org/10.5194/gmd-11-3587-2018>, 2018.
- Rosenthal, Y. and Broccoli, A. J.: In search of Paleo-ENSO, *Science*, 304, 219–221, 2004.
- Roy, T., Lombard, F., Bopp, L., and Gehlen, M.: Projected impacts of climate change and ocean acidification on the global biogeography of planktonic Foraminifera, *Biogeosciences*, 12, 2873–2889, <https://doi.org/10.5194/bg-12-2873-2015>, 2015.
- Sadekov, A., Eggins, S. M., De Deckker, P., and Kroon, D.: Uncertainties in seawater thermometry deriving from intratest and intertest Mg/Ca variability in *Globigerinoides ruber*: Uncertainties Mg/Ca seawater thermometry *Paleoceanography*, 23, PA1215, <https://doi.org/10.1029/2007PA001452>, 2008.
- Sadekov, A., Eggins, S. M., De Deckker, P., Ninnemann, U., Kuhnt, W., and Bassinot, F.: Surface and subsurface seawater temperature reconstruction using Mg/Ca microanalysis of planktonic foraminifera *Globigerinoides ruber*, *Globigerinoides sacculifer*, and *Pulleniatina obliquiloculata*: Seawater temperature reconstruction, *Paleoceanography*, 24, PA3201, <https://doi.org/10.1029/2008PA001664>, 2009.
- Sadekov, A. Y., Ganeshram, R., Pichevin, L., Berdin, R., McClymont, E., Elderfield, H., and Tudhope, A. W.: Palaeoclimate reconstructions reveal a strong link between El Niño–Southern Oscillation and Tropical Pacific mean state, *Nat. Commun.*, 4, 2692, <https://doi.org/10.1038/ncomms3692>, 2013.
- Schiebel, R., Barker, Stephen, Lendt, R., Thomas, H., and Bollmann, J.: Planktic foraminiferal dissolution in the twilight zone, *Deep-Sea Res. Pt. II* 54, 676–686, <https://doi.org/10.1016/j.dsr2.2007.01.009>, 2007.
- Seierstad I. K., Abbott, P. M., Bigler, M., Blunier, T., Bourne, A. J., Brook, E., Buchardt, S. L., Buizert, C., Clausen, H. B., Cook, E., Dahl-Jensen, D., Davies, S. M., Guillevic, M., Johnsen, S. J., Pedersen, D. S., Popp, T. J., Rasmussen, S. O., Severinghaus, J. P., Svensson, A., and Vinther, B. M.: Consistently dated records from the Greenland GRIP, GISP2 and NGRIP ice cores for the past 104 ka reveal regional millennial-scale  $\delta^{18}\text{O}$  gradients with possible Heinrich event imprint, *Quaternary Sci. Rev.*, 106, 29–46, <https://doi.org/10.1016/j.quascirev.2014.10.032>, 2014.
- Spero, H. J. and DeNiro, M. J.: The influence of symbiont photosynthesis on the  $\delta^{18}\text{O}$  and  $\delta^{13}\text{C}$  values of planktonic foraminiferal shell calcite, *Symbiosis*, 4, 213–228, 1987.
- Spero, H. J. and Lea, D. W.: Experimental determination of stable isotope variability in *Globigerina bulloides*: implications for paleoceanographic reconstructions, *Mar. Micropaleontol.*, 28, 231–246, [https://doi.org/10.1016/0377-8398\(96\)00003-5](https://doi.org/10.1016/0377-8398(96)00003-5), 1996.
- Spero, H. J., Bijma, J., Lea, D. W., and Bemis, B. E.: Effect of seawater carbonate concentration on foraminiferal carbon and oxygen isotopes, *Nature*, 390, 497–500, <https://doi.org/10.1038/37333>, 1997.
- Steinhardt, J., Cléroux, C., de Nooijer, L. J., Brummer, G.-J., Zahn, R., Ganssen, G., and Reichert, G.-J.: Reconciling single-chamber Mg/Ca with whole-shell  $\delta^{18}\text{O}$  in surface to deep-dwelling planktonic foraminifera from the Mozambique Channel, *Biogeosciences*, 12, 2411–2429, <https://doi.org/10.5194/bg-12-2411-2015>, 2015.
- Stott, L., Poulsen, C., Lund, S., and Thunell, R.: Super ENSO and Global Climate Oscillations at Millennial Time Scales, *Science*, 297, 222, <https://doi.org/10.1126/science.1071627>, 2002.
- Sverdrup, H. U., Johnson, M. W., and Fleming, R. H.: *The Oceans, Their Physics, Chemistry, and General Biology*, Prentice-Hall, New York, 1942.
- Thirumalai, K., Partin, J. W., Jackson, C. S., and Quinn, T. M.: Statistical constraints on El Niño Southern Oscillation reconstructions using individual foraminifera: A sensitivity analysis, *Paleoceanography*, 28, 401–412, <https://doi.org/10.1002/palo.20037>, 2013.
- Thunell, R. C., Kier, R. S., and Honjo, S.: Calcite dissolution: an in-situ study in the Panama Basin, *Science*, 212, 659–661, 1981.
- Trenberth, K. E. and Otto-Bliesner, B. L.: Toward Integrated Reconstruction of past Climates, *Science*, 300, 589–591, 2003.
- van Sebille, E., Scussolini, P., Durgadoo, J. V., Peeters, F. J. C., Biastoch, A., Weijer, W., Turney, C., Paris, C. B., and Zahn R.: Ocean currents generate large footprints in marine palaeoclimate proxies, *Nat. Commun.*, 6, 6521, <https://doi.org/10.1038/ncomms7521>, 2015.
- Vetter, L., Kozdon, R., Mora, C. I., Eggins, S. M., Valley, J. W., Hönisch, B., and Spero, H. J.: Micron-scale intrashell oxygen isotope variation in cultured planktic

- foraminifers, *Geochim. Cosmochim. Ac.*, 107, 267–278, <https://doi.org/10.1016/j.gca.2012.12.046>, 2013.
- Waelbroeck, C., Mulitza, S., Spero, H., Dokken, T., Kiefer, T., and Cortijo, E.: A global compilation of late Holocene planktonic foraminiferal  $\delta^{18}\text{O}$ : relationship between surface water temperature and  $\delta^{18}\text{O}$ , *Quaternary Sci. Rev.*, 24, 853–868, 2005.
- Wang, C., Deser, C., Yu, J.-Y., DiNezio, P., and Clement, A.: El Niño and Southern Oscillation (ENSO): A Review, in: *Coral Reefs of the Eastern Tropical Pacific: Persistence and Loss in a Dynamic Environment*, edited by: Glynn, P. W., Manzello, D. P., and Enochs, I. C., Springer Netherlands, Dordrecht, 85–106, 2017.
- Wang, X. L.: The Coupling of the Annual Cycle and ENSO Over the Tropical Pacific, *J. Atmos. Sci.*, 51, 1115–1136, [https://doi.org/10.1175/1520-0469\(1994\)051<1115:TCOTAC>2.0.CO;2](https://doi.org/10.1175/1520-0469(1994)051<1115:TCOTAC>2.0.CO;2), 1994.
- Waterson, A. M., Edgar, K. M., Schmidt, D. N., and Valdes, P. J.: Quantifying the stability of planktic foraminiferal physical niches between the Holocene and Last Glacial Maximum, *Paleoceanography*, 32, 74–89, <https://doi.org/10.1002/2016PA002964>, 2016.
- Wessel, P. and Lyons, S.: Distribution of large Pacific seamounts from Geosat/ERS-1, *J. Geophys. Res.*, 102, 459–475, 1997.
- Weyl, P. K.: Micropaleontology and Ocean Surface Climate, *Science*, 202, 475–481, 1978.
- White, S. M., Ravelo, A. C., and Polissar, P. J.: Dampened El Niño in the Early and Mid-Holocene Due to Insolation-Forced Warming/Deepening of the Thermocline, *Geophys. Res. Lett.*, 45, 316–326, <https://doi.org/10.1002/2017GL075433>, 2018.
- Wilke, I., Bickert, T., and Peeters, F. J. C.: The influence of seawater carbonate ion concentration  $[\text{CO}_3^{2-}]$  on the stable isotope composition of planktic foraminifera species *Globorotalia inflata*, *Mar. Micropaleontol.*, 58, 243–258, <https://doi.org/10.1016/j.marmicro.2005.11.005>, 2006.
- Wit, J. C., Reichert, G. J., and Ganssen, G. M.: Unmixing of stable isotope signals using single specimen  $\delta^{18}\text{O}$  analyses, *Geochim. Geophys. Geos.*, 14, 1312–1320, <https://doi.org/10.1002/ggge.20101>, 2013.
- Wolf-Gladrow, D. A., Bijma, J., and Zeebe, R. E.: Model simulation of the carbonate chemistry in the microenvironment of symbiont bearing foraminifera, *Mar. Chem.*, 64, 181–198, [https://doi.org/10.1016/S0304-4203\(98\)00074-7](https://doi.org/10.1016/S0304-4203(98)00074-7), 1999.
- Wunsch, C.: On sharp spectral lines in the climate record and the millennial peak, *Paleoceanography*, 15, 417–424, <https://doi.org/10.1029/1999PA000468>, 2000.
- Wunsch, C. and Gunn, D. E.: A densely sampled core and climate variable aliasing, *Geo-Mar. Lett.*, 23, 64–71, <https://doi.org/10.1007/s00367-003-0125-2>, 2003.
- Wycech, J. B., Kelly, D. C., Kitajima, K., Kozdon, R., Orland, I. J., and Valley, J. W.: Combined effects of gametogenic calcification and dissolution on  $\delta^{18}\text{O}$  measurements of the planktic foraminifer *Trilobatus sacculifer*, *Geochem. Geophys. Geosyst.*, 19, 4487–4501, <https://doi.org/10.1029/2018GC007908>, 2018.
- Xie, S.-P.: On the Genesis of the Equatorial Annual Cycle, *J. Climate*, 7, 2008–2013, 1994.
- Xie, S.-P.: Interaction between the annual and interannual variations in the equatorial Pacific, *J. Phys. Oceanogr.*, 25, 1930–1941, 1995.
- Žarić, S., Donner, B., Fischer, G., Mulitza, S., and Wefer, G.: Sensitivity of planktic foraminifera to sea surface temperature and export production as derived from sediment trap data, *Mar. Micropaleontol.*, 55, 75–105, <https://doi.org/10.1016/j.marmicro.2005.01.002>, 2005.
- Žarić, S., Schulz, M., and Mulitza, S.: Global prediction of planktic foraminiferal fluxes from hydrographic and productivity data, *Biogeosciences*, 3, 187–207, <https://doi.org/10.5194/bg-3-187-2006>, 2006.
- Zebiak, S. E. and Cane, M. A.: A Model El Niño-Southern Oscillation, *Mon. Weather Rev.*, 115, 2262–2278, [https://doi.org/10.1175/1520-0493\(1987\)115<2262:AMENO>2.0.CO;2](https://doi.org/10.1175/1520-0493(1987)115<2262:AMENO>2.0.CO;2), 1987.
- Zeebe, R. E. and Sanyal, A.: Comparison of two potential strategies of planktonic foraminifera for house building:  $\text{Mg}^{2+}$  or  $\text{H}^+$  removal?, *Geochim. Cosmochim. Ac.*, 66, 1159–1169, [https://doi.org/10.1016/S0016-7037\(01\)00852-3](https://doi.org/10.1016/S0016-7037(01)00852-3), 2002.
- Zhu, J., Liu, Z., Brady, E., Otto-Bliesner, B., Zhang, J., Noone, D., Tomas, R., Nusbaumer, J., Wong, T., Jahn, A., and Tabor, C.: Reduced ENSO variability at the LGM revealed by an isotope-enabled Earth system model, *Geophys. Res. Lett.*, 44, 6984–6992, <https://doi.org/10.1002/2017GL073406>, 2017.